Endocytic Patch Dynamics are Differentially Regulated at Distinct Cell Sites in Fission Yeast

Bethany F. Campbell[1], Uma J. Patel[1], Ashlei R. Williams[2], and Maitreyi E. Das[1]*

[1]Boston College, Chestnut Hill, MA

[2]The University of Tennessee, Knoxville, TN

Correspondence: *dasma@bc.edu

Running Title: Cdc42 regulates branched actin

Keywords: Polarization, Branched Actin Networks, Clathrin-mediated Endocytosis, Cdc42 GTPase, p21-Activated Kinase, Type I Myosin

ABSTRACT

Endocytosis promotes polarity and growth in eukaryotes. In *Schizosaccharomyces pombe* fission yeast, endocytosis occurs at the polarized cell ends and division site and at the non-polarized cell sides. Our characterization of endocytic actin patches show that they are differentially regulated. The patches at the cell ends and division site internalize successfully while those at the sides are weak and erratic. The major regulator of cell polarity, Cdc42, and its target Pak1 kinase only localize to the cell ends and division site. We find that these proteins regulate assembly and internalization of patches at these sites but not at the cell sides. Moreover, Cdc42 specifically activated by the GEF Gef1 promotes proper patch dynamics. Endocytosis requires phosphorylation of the Type I Myosin Myo1 by the Pak1 kinase. Myo1 localizes to the cell ends, division site, and the cell sides. We find that unlike Cdc42 and Pak1, Myo1 also promotes patch assembly at the cell sides. Our data indicate that while Myo1 can globally promote branched actin assembly, successful endocytic patch dynamics and internalization at polarized sites require Cdc42 and Pak1 kinase.

SUMMARY STATEMENT

Endocytic patch dynamics are differentially regulated at distinct sites such as the cell ends, division site and the cell sides by Cdc42 and its downstream targets Pak1 kinase and the Type 1 myosin.

INTRODUCTION

Endocytosis is an essential process by which cells uptake nutrients and recycle proteins from the plasma membrane. In cell-walled organisms such as the fission yeast *Schizosaccharomyces pombe*, internal turgor pressure is high at ~10 atm (Basu et al., 2014; Lacy et al., 2018), roughly equivalent to a racing bike tire. To overcome such high turgor pressure, successful clathrin-mediated endocytosis in yeasts requires synthesis of branched actin networks to produce enough counteractive force to invaginate the plasma membrane and subsequently internalize endocytic vesicles (Aghamohammadzadeh and Ayscough, 2009; Basu et al., 2014; Nickaeen et al., 2022). In *S. pombe*, branched actin is formed by the Arp2/3 complex with the help of nucleation promoting factors such as the Type I myosin Myo1 and the WASP Wsp1 (Sirotkin et al., 2005). Actin binding proteins such as fimbrin Fim1 also localize to endocytic patches to crosslink the branched actin and stimulate force production within the patch (Skau et al., 2011). Furthermore, if endocytosis is impaired, cells cannot grow or divide. Once treated with the Arp2/3 complex inhibitor, CK-666, *S. pombe* cells halt their growth during interphase and fail to form a septum during cytokinesis (Onwubiko et al., 2019). Thus, regulation of branched actin formation is an essential cellular process for *S. pombe* cell viability.

In rod-shaped *S. pombe* cells, clathrin-mediated endocytic events primarily occur at sites of polarization, namely the cell ends during interphase and the division site during cytokinesis (Gachet and Hyams, 2005; Sirotkin et al., 2010). However, some endocytic actin patches also form at the non-growing cell sides. Previous work has shown that sites of endocytosis coincide with regions of cell growth and cytokinesis (Gachet and Hyams, 2005). The GTPase Cdc42 is the major regulator of polarity in *S. pombe* and is active only at polarized cell ends and the division site and not at the cell sides (Das et al., 2012). Additionally, Cdc42 is activated at the division site during actomyosin ring formation and persists throughout cytokinesis (Hercyk and

59 Das, 2019a; Wei et al., 2016). Further work has connected Cdc42 activation to Arp2/3-mediated
60 endocytosis since both are required for septum formation and onset of actomyosin ring
61 constriction in fission yeast (Campbell et al., 2022; Onwubiko et al., 2019). Studies in
62 mammalian MDCK cells also indicate that Cdc42 regulates both endocytic trafficking and
63 exocytic secretion (Kroschewski et al., 1999). Specifically, expression of dominant negative
64 $Cdc42^{T17N}$ mislocalizes basolateral membrane proteins to the apical membrane, while
65 expression of constitutively active Cdc42Q61L depolarizes actin from the apical membrane,
66 causing actin to instead appear throughout the cell periphery (Kroschewski et al., 1999).
67 In *S. pombe*, Cdc42 is independently activated by two GEFs, a transient and mostly cytoplasmic
68 GEF, Gef1, which localizes to cortical puncta at polarized regions (Coll et al., 2003; Das et al.,
69 2015; Hercyk and Das, 2019b), as well as a strong GEF, Scd1, which localizes throughout
70 polarized regions and promotes sustained Cdc42 activation via a positive feedback loop (Das et
71 al., 2012; Das and Verde, 2013; Lamas et al., 2020). Like Cdc42, both of these GEFs are
72 present at polarized cell ends, but it remains unclear which one arrives first at this site to initiate
73 Cdc42 activation, although Scd1 has been shown to prevent ectopic localization of Gef1
74 (Hercyk et al., 2019). Previous research has shown that Gef1 is recruited to cortical patches via
75 the F-BAR protein Cdc15 (Hercyk and Das, 2019a; Hercyk and Das, 2019b), which promotes
76 endocytosis and is itself recruited to endocytic actin patches via the endocytic Type I myosin,
77 Myo1 (Arasada and Pollard, 2011; Carnahan and Gould, 2003). Conversely, Cdc15 does not
78 recruit Scd1 to cortical patches (Hercyk and Das, 2019b). Additionally, loss of *gef1* leads to
79 excessive accumulation and prolonged lifetimes of Cdc15 within endocytic patches, which can
80 be rescued by expression of a constitutively active *cdc42G12V* allele (Adams et al., 1990).
81 Together, these reports suggest that Cdc15 recruits Gef1 to endocytic patches to promote
82 Cdc42 activation and that this recruitment is important to regulate endocytic patch dynamics.
83

84 Prior research has additionally linked Cdc42 activity to the regulation of endocytosis via its direct
85 downstream effector, the p21-activated kinase (PAK) (Murray and Johnson, 2001; Ottilie et al.,
86 1995; Wu et al., 1997), which is activated by binding GTP-bound Cdc42 to relieve its
87 autoinhibition (Bokoch, 2003). Like Cdc42, PAK is conserved across eukaryotic life from yeast
88 to humans, functioning as a serine/threonine kinase (Manser et al., 1994; Marcus et al., 1995).
89 In unicellular eukaryotes, PAK is known to phosphorylate the endocytic Type I myosin in
90 organisms such as slime molds, amoebas, and yeasts (Brzeska et al., 1997; Lechler et al.,
91 2001; Lechler et al., 2000; Lee et al., 2000; Murray and Johnson, 2001; Wu et al., 1997),
92 including *S. pombe* (Attanapola et al., 2009). In these organisms, PAK promotes the ATPase
93 activity and motor function of the Type I myosin by phosphorylating a conserved serine or
94 threonine residue located in the motor domain known as the TEDS-site (Bement and Mooseker,
95 1995; Fujita-Becker et al., 2005; Pedersen et al., 2023). Specifically, TEDS-site phosphorylation
96 facilitates association of the myosin with actin, stabilizing the complex (Fujita-Becker et al.,
97 2005). In *S. pombe*, phospho-null mutation of the TEDS-site abrogates proper localization of
98 Myo1 to endocytic actin patches, instead causing the myosin to localize uniformly along the
99 plasma membrane (Attanapola et al., 2009). Additionally, we have recently shown that Pak1
100 promotes successful internalization of endocytic patches and even its own removal via
101 endocytosis at growing cell ends of *S. pombe* (Harrell et al., 2024). These findings suggest that
102 regulation of Cdc42 activation may be necessary to facilitate proper endocytic patch dynamics.
103
104 While we see distinct sites of endocytosis at the cells ends, division site, and the cell sides, it is
105 not known whether these sites are functionally similar and if they show different regulatory
106 patterns. Here, we use genetic approaches and quantitative live cell imaging to better define the
107 intricate connections between the different sites of polarization and endocytosis. We show that
108 endocytic actin patches display disparate dynamics at distinct cell sites. Endocytosis at the
109 polarized sites requires Cdc42, its target Pak1, and the downstream substrate Myo1. At the cell

110 sides, Myo1 but not Cdc42 and Pak1 regulates patch assembly and dynamics. While our recent
111 work shows that endocytosis ensures proper spatiotemporal regulation of Cdc42 activation
112 (Harrell et al., 2024), here we demonstrate that Cdc42 activation likewise spatiotemporally
113 directs endocytosis.

RESULTS

Endocytic events at distinct regions in the cell show differential dynamics

To our knowledge, the dynamic behaviors of individual endocytic patches within each distinct region have not been characterized and reported. We were thus curious to determine how endocytic patches at polarized regions behave compared to those at non-growing regions. To do this, we performed 1-sec interval timelapse imaging of asynchronous cultures of wild-type cells expressing mEGFP-tagged fimbrin Fim1, a branched actin crosslinker (Nakano et al., 2001), which promotes actin bundling necessary for endocytic patch internalization (Skau et al., 2011). This approach allowed us to simultaneously capture the dynamics of individual endocytic patches at the cell ends, the cell sides, and the division site (Fig. 1 A). We then used the FIJI plugin TrackMate (Tinevez et al., 2017) to track the trajectories of individual Fim1-mEGFP patches. From this data, we found that Fim1-mEGFP-labeled endocytic patches have disparate lifetimes at each region, with patches at the cell sides exhibiting the shortest lifetimes, while patches at the division site show the longest lifetimes (Fig. 1 B). While the lifetimes at polarized cell ends and the division site are statistically different in duration, the mean lifetimes for both regions (~16 sec at the cell ends and ~18 sec at the division site) fall within the reported average range for Fim1-mEGFP lifetimes (Berro and Pollard, 2014; Sirotkin et al., 2010). In contrast, the patch lifetime at the cell sides is ~12 sec (Fig. 1 B), well below than that at the polarized sites.

Mean patch intensity was also measured frame-by-frame throughout each patch's lifetime. This analysis revealed that endocytic patches at the cell ends and the division site recruit Fim1-mEGFP at the same rate and to the same peak intensity (Fig. 1 C). Conversely, endocytic patches at the cell sides recruited ~50% less Fim1-mEGFP at peak intensity compared to the polarized sites (Fig. 1 C). Using the R package TrackMateR (Sittewelle and Royle, 2024) , we

139 calculated the diffusive properties of tracked Fim1-mEGFP patches to characterize their
140 respective dynamics. Calculations show that endocytic patches at the division site are the
141 slowest moving (Fig. 1 D) and most stable with the least diffusion of all sites (Fig. 1 F). In
142 contrast, endocytic patches at the cell sides move the fastest (Fig. 1 D) and exhibit the highest
143 diffusion rate (Fig. 1 F). Patches at the cell ends display a comparatively intermediate speed
144 and diffusion rate (Fig. 1 D and F). However, mean squared displacement (MSD) analysis
145 reveals that endocytic patches at the cell ends and the division site exhibit similar degrees of
146 directed motion, while patches at the cell sides demonstrate more diffusive behavior overall
147 (Fig. 1 E). Together, these data indicate that endocytic patches at polarized regions recruit twice
148 as much Fim1-mEGFP, are longer-lived, and exhibit more stable and directed dynamics
149 compared to patches at the non-growing cell sides.

150 **Cdc42 activity promotes timely formation of endocytic branched actin networks at the**
151 **division site**

152 Our findings that endocytic events behave differently at polarized regions compared to non-
153 growing cell sides suggest that polarity regulators may influence endocytic dynamics. Indeed,
154 Cdc42 has been shown to promote uptake of Lucifer Yellow via endocytosis in *S. pombe*
155 (Murray and Johnson, 2001). Connecting previous observations that sites of endocytosis mirror
156 sites of Cdc42 activation, we asked if Cdc42 activation is necessary for endocytosis. To test this
157 idea, we asked if a delay in Cdc42 activation at the division site would consequently delay onset
158 of endocytic activity within the division plane. We selected the division site since the temporal
159 pattern of Cdc42 activation is best understood at this site. The GEF Gef1 is the first GEF to
160 appear and activate Cdc42 at the division site, and loss of Gef1 consequently leads to a delay in
161 Cdc42 activity at this site (Wei et al., 2016) since the other Cdc42 GEF, Scd1, depends on
162 Gef1 for timely localization to the division site (Hercyk et al., 2019). While delayed Cdc42
163 activation in *gef1Δ* mutant delays actomyosin ring constriction due to delayed recruitment of
164 Bgs1, the timing of mitotic events proceeds normally (Wei et al., 2016). Thus, we measured the
165 timing of Fim1-mEGFP appearance at the division site relative to onset of mitosis marked by
166 spindle pole body (SPB) separation in *gef1Δ* cells compared to *gef1*$^{+}$ controls. These
167 experiments show that Fim1-mEGFP first appears at the division site ~12 mins after SPB
168 separation in *gef1*$^{+}$ cells, while its appearance in *gef1Δ* cells is delayed to ~20 mins post-SPB
169 separation (green dotted box, Fig. 2A and Supplementary Fig.S1A). Intriguingly, Cdc42 is also
170 first activated at the division site ~10-12 min post-SPB separation in wild-type cells (Hercyk and
171 Das, 2019b; Wei et al., 2016). Fim1-mEGFP patches appear uniformly throughout the division
172 site ~20 mins post-SPB separation in *gef1*$^{+}$ controls compared to ~28 mins post-SPB separation
173 in *gef1Δ* mutants (solid green box, Fig. 2 A and B). These findings suggest that Cdc42
174 activation is indeed required for endocytosis.

175 We were then curious to determine how long after Cdc42 activation does Fim1 appear at the
176 division site in *gef1*$^{+}$ as well as *gef1Δ* cells. In *gef1*$^{+}$ cells, Fim1-mCherry first appears at the
177 division site (purple dotted box) ~5-6 mins after Cdc42 is activated (green box and arrowheads,
178 Fig. 2 D and Supplementary Fig.S1B), as visualized by the CRIB-3xGFP bio-probe which binds
179 active GTP-bound Cdc42 (Tatebe et al., 2008). Comparatively, in *gef1Δ* cells, Fim1-mEGFP first
180 appears at the division site (purple dotted box) about the same time as Cdc42 activation (green
181 box and arrowheads, Fig. 2 D and Supplementary Fig.S1B). Similarly, Fim1-mCherry appears
182 throughout the division site after Cdc42 activation at ~7-8 mins in *gef1*$^{+}$ and at ~4 mins in *gef1Δ*
183 cells (Fig. 2 C and D). This suggests that endocytosis starts soon after Cdc42 activation in
184 *gef1Δ* mutants since these cells have already progressed through mitosis and thus many
185 cellular events are already complete. Our findings suggest that *gef1Δ* cells simply await Cdc42
186 activation to initiate endocytosis. Together, these data suggest that Cdc42 activation is required
187 for the onset of endocytosis at the division site.

188 **The GEFs Gef1 and Scd1 differentially regulate Cdc42 to direct branched actin synthesis**
189 **and dynamics at sites of polarization**
190 While the Cdc42 GEF Scd1 is required for polarized growth at the cell ends, Gef1 is required for
191 bipolar growth (Hercyk et al., 2019). Findings that Gef1 and Scd1 differentially activate Cdc42 at
192 polarized sites prompted us to define the manner of Cdc42 activation required to direct
193 endocytosis. We tracked the dynamics of Fim1-mEGFP at the ends in *gef1Δ* and *scd1Δ* cells
194 compared to *gef1*$^{+}$*scd1*$^{+}$ controls, as previously described (Fig. 1). In these experiments, cells
195 also expressed Cdc15-tdTomato to corroborate and expand upon our previous findings. As
196 shown before (Onwubiko et al., 2019), *gef1Δ* mutants exhibit excessive accumulation and
197 prolonged lifetimes of Cdc15-tdTomato at the cell ends compared to *gef1*$^{+}$ control cells (Fig. 3
198 A; Supplementary Fig. S2 A and B). We additionally find that Fim1-mEGFP accumulation within
199 endocytic patches is likewise increased in *gef1Δ* mutants at both the cell ends and the division
200 site compared to controls. (Fig. 3 A, B, and D). In in *gef1Δ* mutants, Fim1-mEGFP lifetimes are
201 also prolonged at the cell ends; however, we saw no change in patch lifetime at the division site
202 in *gef1Δ* cells (Fig. 3 H). Notably, the recruitment patterns and lifetimes of Fim1-mEGFP
203 patches are the same at the cell sides of *gef1*$^{+}$ and *gef1Δ* cells (Fig. 3 F and H), which suggests
204 that the dynamics of these patches are not influenced by Cdc42 or its GEFs.
205
206 In contrast, in *scd1Δ* mutants, we did not observe any change in the recruitment dynamics of
207 either Cdc15-tdTomato or Fim1-mEGFP compared to *scd1*$^{+}$ cells (Supplementary Fig. S2 C and
208 D; Fig. 3 A, C, E, and G). We did, however, find that Fim1-mEGFP patches are depolarized
209 rather than concentrated at the cell ends in *scd1Δ* mutants (Supplementary Fig. S2 E). Fim1-
210 mEGFP patches in *scd1Δ* mutants also display similar lifetimes at all regions of the cell (Fig. 3
211 H), which is consistent with the random, depolarized Cdc42 activation patterns that occur in
212 these cells due to loss of Scd1-mediated restriction of ectopic Gef1 localization (Hercyk et al.,

213 2019). Together, these results suggest that Gef1 is the primary GEF that regulates Cdc42

214 activation to direct proper endocytic patch dynamics at polarized regions.

215 **Pak1/Orb2 kinase activity promotes timely formation of endocytic branched actin**
216 **networks at the division site**
217 Next, we asked if Cdc42 regulates endocytosis via its target the Pak1 kinase. In addition to the
218 cell ends, Pak1 is also present at the division site during cytokinesis where it promotes
219 assembly of the contractile actomyosin ring (Magliozzi et al., 2020). Similar to previously
220 described experiments (Fig. 2), we measured the time intervals between SPB separation and
221 appearance of Fim1-mEGFP at the division site in *orb2*$^{+}$ cells compared to *orb2-34*, a kinase-
222 dead, temperature-sensitive allele of *pak1* (Das et al., 2012; Verde et al., 1995). Even at
223 permissive temperature, *orb2-34* mutants show minimal kinase activity and display polarity
224 defects compared to wild-type *pak1* (Das et al., 2012; Verde et al., 1995). Thus, experiments
225 were performed under permissive 25°C conditions to minimize pleiotropic effects that may arise
226 under temperature restriction, which causes *orb2-34* cells to become rounded and orb-like
227 (Verde et al., 1995). Under permissive conditions, the *orb2-34* mutants grow as well as *orb2*$^{+}$
228 cells and only display cell morphology defects. Nevertheless, we do see a ~2 min delay in the
229 appearance of Fim1-mEGFP appearance (dotted and solid green boxes) at the division site in
230 *orb2-34* mutants compared to controls (Fig. 4 A-C). While this is not a major delay, it is
231 consistent and significant. It is possible that under complete abrogation of Pak1 kinase activity
232 the difference will be enhanced. However, our experimental conditions do not allow us to
233 expose the cells to such extreme conditions for extended timelapse imaging while avoiding
234 pleiotropic effects. Thus, these data indicate that timely initiation of endocytosis at the division
235 site depends both on Cdc42 and Pak1 activation.

236 **Pak1 facilitates proper formation and dynamics of endocytic actin patches at sites of**
237 **polarization**
238
239 Given our recent findings that loss of Pak1 kinase function impairs internalization of endocytic
240 patches at polarized cell ends (Harrell et al., 2024), we asked whether similar endocytic defects
241 also occur at the division site and cell sides. To examine this, we tracked Fim1-mEGFP patches
242 in temperature-sensitive *orb2-34* mutants and compared their dynamics to patches tracked in
243 *orb2*$^{+}$ control cells. As at the cell ends (Harrell et al., 2024), Fim1-mEGP patch internalization at
244 the division site is impaired in *orb2-34* mutants compared to controls, especially at the 35°C
245 restrictive temperature (Fig. 5 A). Overall, it appears that Fim1 patches largely move within the
246 plane of the plasma membrane in the absence of Pak1 kinase function.
247
248 We also observe impaired recruitment of Fim1-mEGFP to endocytic patches in *orb2-34* mutants
249 under permissive conditions. At 25°C, *orb2-34* cells show decreased peak Fim1-mEGFP
250 intensity within endocytic patches at the cell ends and the division site compared to controls
251 (Fig. 5 B and D). In contrast, at the 35°C restrictive temperature, peak Fim1-mEGFP intensity at
252 the cell ends in *orb2-34* mutants remains the same as observed at 25°C, while *orb2*$^{+}$ controls
253 show decreased Fim1-mEGFP patch intensity at the cell ends at this temperature (Fig. 5 C).
254 However, we observe the opposite effect at the division site. Here at 35°C, Fim1-mEGFP patch
255 intensity dramatically decreases at the division site in *orb2-34* mutants while patch intensity is
256 unchanged in *orb2*$^{+}$ controls (Fig. 5 E). These observations suggest that Fim1 recruitment to the
257 cell ends of *orb2-34* mutants is insensitive to temperature restriction, while Fim1 recruitment to
258 the division site of *orb2-34* mutants is impaired under these conditions. Given that patch
259 internalization is impaired at the cell ends in *orb2-34* mutants (Harrell et al., 2024), our data
260 suggest the level of actin assembly and dynamics alone do not determine the ability of
261 endocytic vesicles to successfully internalize. Consistent with previous experiments showing

262 that endocytic dynamics at the cell sides are not influenced by changes in polarity regulation, we
263 did not observe changes in Fim1-mEGFP recruitment at these sites other than some decrease
264 in peak patch intensity in *orb2*$^{+}$ controls at 35°C (Fig. 5 F and G).
265
266 Across the board at all cell regions, Fim1-mEGFP patch lifetimes decrease at 35°C compared to
267 25°C (Fig. 5 H and I), likely due to increased Brownian motion. As previously reported (Harrell et
268 al., 2024), Fim1-mEGFP patch lifetimes do not change at the cell ends of *orb2-34* mutants
269 compared to controls (Fig. 5 H and I). Conversely, at 25°C, Fim1-mEGFP patch lifetimes are ~5
270 seconds shorter at the division site in *orb2-34* cells compared to *orb2*$^{+}$ cells (Fig. 5 H), but this
271 difference is abrogated at 35°C where *orb2*$^{+}$ patch lifetimes decrease (Fig. 5 I). While loss of
272 Pak1 kinase function impairs endocytic internalization at both the cell ends and the division site,
273 our data suggests that Pak1 may perform additional functions at the division site since we
274 observe changes in Fim1 accumulation and lifetime at this site, but not at the cell ends.
275 Together, these results indicate that Pak1 kinase plays important and differential roles at
276 polarized regions to regulate endocytic patch behavior.

277 **The Type I myosin Myo1 promotes timely internalization of endocytic actin patches via**
278 **Pak1-mediated phosphorylation of its motor domain**

279 Our data show that endocytosis is differentially regulated at distinct sites within polarized cells.
280 While Cdc42 and Pak1 kinase are required for proper actin patch dynamics at the cell ends and
281 the division site, they are not required for the patches at the cell sides. Given that previous
282 reports indicate that the Pak1 kinase regulates endocytosis via Myo1 phosphorylation, we asked
283 if Myo1 itself is differentially required for endocytosis at these distinct sites. We first analyzed
284 Myo1-GFP localization in *S. pombe*. As expected Myo1-GFP localizes to the growing cell ends
285 and the division site (Attanapola et al., 2009; Carnahan and Gould, 2003; Lee et al., 2000).
286 Myo1-GFP puncta also appear along the cell sides, co-localizing with branched actin patches as
287 labeled with Fim1-mCherry (arrowheads, Supplementary Fig. S3A) (Arasada and Pollard, 2011;
288 Sirotkin et al., 2010). Next, we examined Fim1 dynamics in *myo1Δ* cells compared to *myo1*$^{+}$
289 controls at the cell ends, division site, and the cell sides. In the absence of *myo1*, endocytic
290 patches marked with Fim1-mCherry display weak internalization and largely slide within the
291 plane of the plasma membrane at both the cell ends and the division site (Fig. 6 A). Additionally,
292 fewer endocytic patches form in *myo1Δ* mutants, although Fim1-mCherry lifetimes are much
293 longer compared to controls at all regions (Fig. 6 B). Notably, while Fim1-mCherry recruitment
294 to endocytic patches reaches higher peak levels in *myo1Δ* cells compared to *myo1*$^{+}$ controls,
295 Fim1 takes longer to accumulate at patches in these mutants (Fig. 6 D). Indeed, peak Fim1-
296 mCherry patch intensity is reached ~8 seconds later at the cell ends (Fig. 6 E) and ~11 seconds
297 later at the division site in *myo1Δ* mutants compared to *myo1*$^{+}$ controls due to this slower
298 recruitment of Fim1 (Fig. 6 F). At the cell sides, peak Fim1-mCherry patch intensity is slightly
299 increased in *myo1Δ* cells and patches also take longer to reach peak intensity (Fig. 6 G). Since
300 Myo1 can localize to cell sides in addition to sites of polarization, this may explain the changes
301 in Fim1 behavior at the cell sides in *myo1Δ* mutants.

302

303 While Pak1 phosphorylates Myo1 at the S361 TEDS site located within its N-terminal motor
304 domain (Attanapola et al., 2009), Myo1 also binds and weakly activates the branched actin
305 nucleating Arp2/3 complex via its C-terminal tail (Lee et al., 2000; Sirotkin et al., 2005). Thus,
306 Myo1 may promote endocytic patch internalization via its N-terminal motor function and/or its C-
307 terminal association with Arp2/3. As *myo1Δ* completely abolishes all Myo1 function,
308 experiments in *myo1Δ* mutants alone cannot distinguish between these mechanistic
309 possibilities. To determine if Pak1-mediated Myo1 phosphorylation is necessary to promote
310 endocytic patch internalization, we examined endocytic patch behavior in the single point TEDS
311 site phospho-null mutant, *myo1-S361A*, which cannot be phosphorylated by Pak1 but retains its
312 C-terminal Arp2/3 binding domain (Attanapola et al., 2009). In the absence of Pak1-mediated
313 phosphorylation of Myo1, we hypothesized that Fim1-mCherry patches would show similar
314 weak internalization as observed in *myo1Δ* mutants.

315

316 In the TEDS site *myo1-S361A* mutant, we find that Fim1-mCherry is adequately recruited to
317 endocytic patches, yet the patches do not properly internalize (Fig. 6 A and D, Fig. S2 A and B).
318 Additionally, we observe that Myo1-S361A-GFP intensity remains mostly stable at the plasma
319 membrane of polarized cell ends, while in *myo1*$^{+}$ cells, Myo1-GFP intensity increases as Fim1-
320 mCherry is recruited to endocytic patches and is lost as Fim1-mCherry patches internalize at
321 the cell ends (Fig. S2), as reported previously (Sirotkin et al., 2005). We also observe increased
322 cytoplasmic intensity of Myo1-S361A-GFP compared to controls (Fig. S2 A and B). In *myo1-*
323 *S361A* mutants, Fim1-mCherry lifetimes are indistinguishable from *myo1*$^{+}$ controls at the cell
324 ends and sides, but patch lifetimes are prolonged at the division site (Fig. 6 C). Similar to
325 *myo1Δ* mutants, the timing of Fim1 recruitment to endocytic patches is prolonged in *myo1-*
326 *S361A* mutants (Fig. 6 D and H; Fig. S2). At the division site, Fim1 recruitment is enhanced in
327 *myo1-S361A* mutants and peak Fim1-mCherry intensity is reached slightly later compared to

328 *myo1*$^{+}$ controls (Fig. 6 I), mimicking *myo1Δ* mutants (Fig. 6 F). Similar to *myo1Δ* mutants, peak
329 Fim1-mCherry intensity at the cell ends is reached later in *myo1-S361A* mutants compared to
330 controls (Fig. 6 J). These observations suggest that branched actin formation can occur in the
331 absence of Myo1 function, even though Myo1 is a nucleation promoting factor, albeit weak
332 compared to Wsp1 (Sirotkin et al., 2005). We also find that while Myo1 regulates patch lifetimes
333 at the cell sides, the TEDS site phosphorylation is not required for the patches at these sites.
334 This aligns with the fact that the Pak1 kinase that phosphorylates the TEDS is also not required
335 for patch dynamics at the cell sides.

336 **Cdc42 and Pak1 activity regulate the recruitment and dynamics of Myo1 at polarized sites**

337 Our data show that Cdc42 and Pak1 are required for proper endocytic dynamics at polarized
338 sites. We asked if Cdc42 and Pak1 regulate endocytosis via the regulation of Myo1 recruitment
339 and dynamics at these sites. To test this, we first observed whether loss or delay of Cdc42 or
340 Pak1 activation at the division site delays Myo1 recruitment to this site. Using *gef1Δ* mutants to
341 delay Cdc42 activation at the division site as previously described (Fig. 2), we observe that
342 Myo1-GFP recruitment to the division site is consequently delayed by ~10 mins compared to
343 *gef1*$^{+}$ control cells (Fig. 7 A and B). Similarly, in *orb2-34* mutants lacking Pak1 kinase activity,
344 Myo1-GFP recruitment to the division plane is delayed by ~4 mins compared to *orb2*$^{+}$ controls,
345 even under permissive conditions (Fig. 7 C and D). These findings indicate that both Cdc42 and
346 Pak1 activation promote timely recruitment of Myo1 to the division site.
347
348 Following our findings at the division site, we then asked if Cdc42 and Pak1 activation similarly
349 regulate Myo1 recruitment to polarized cell ends. To test this, we first measured the mean
350 intensity of Myo1-GFP recruited to the cell ends in genotypes with varying degrees of Cdc42
351 activity. While loss of *gef1* decreases Cdc42 activity (Wei et al., 2016), loss of the GAPs *rga4*
352 and *rga6* increases Cdc42 activation levels (Campbell et al., 2022). Thus, we measured mean
353 Myo1-GFP intensity at the cell ends of *gef1Δ* and *rga4Δrga6Δ* mutants compared to control
354 cells. Intriguingly, Myo1-GFP recruitment is decreased in *gef1Δ* mutants and conversely
355 enhanced in *rga4Δrga6Δ* mutants compared to controls (Fig. 8 A and B). To investigate the
356 dynamics of Myo1 at the cell ends, we also performed 1 sec-interval time-lapse imaging and
357 measured the dwell time of Myo1-GFP at the plasma membrane. These analyses reveal that
358 Myo1-GFP dwell time is increased in both *gef1Δ* and *rga4Δrga6Δ* mutants compared to
359 controls, suggesting that the myosin is less dynamic in both cases (Fig. 8 C and D).
360

361 We then performed similar experiments in *orb2-34* cells to see if decreased Pak1 activation
362 impairs Myo1-GFP recruitment and dynamics at cell ends. Under permissive conditions at 25C°,
363 mean Myo1-GFP intensity is indistinguishable between *orb2-34* and *orb2*$^{+}$ cell ends (Fig. 8 E
364 and F). In contrast, temperature restriction at 35C° reduces mean Myo1-GFP intensity at the cell
365 ends in both *orb2*$^{+}$ and *orb2-34* cells, although Myo1-GFP recruitment is more severely
366 impacted in *orb2-34* mutants (Fig. 8 E and F). Finally, loss of Pak1 kinase function likewise
367 impairs Myo1-GFP dynamics at cell ends, as Myo1-GFP dwell times at the plasma membrane
368 are prolonged in *orb2-34* compared to *orb2*$^{+}$ cells under permissive conditions (Fig. 8 G and H).
369 Together, these data indicate that Cdc42 and Pak1 activation promote the recruitment of Myo1
370 to the plasma membrane in a dose-dependent manner. Additionally, these results suggest that
371 an intermediate range of Cdc42 activation facilitates proper Myo1 dynamics. In summary, our
372 findings suggest that sufficient recruitment of Myo1 to polarized sites depends on both Cdc42
373 and Pak1 activation.

374 **DISCUSSION**

375 In many cell-walled organisms, endocytosis is an actin-dependent process since cells must
376 overcome high internal turgor pressure to properly bend and invaginate the plasma membrane
377 (Basu et al., 2014; Lacy et al., 2018). In yeast, branched actin polymerization and crosslinking
378 provide the force needed to promote successful patch internalization against high turgor
379 pressure (Basu et al., 2014; Kaksonen and Roux, 2018; Skau et al., 2011). However, it is not
380 known whether the force requirements are the same at distinct sites of endocytosis. For
381 instance, at the division site, patches form in close proximity to the actomyosin ring, the
382 synthesizing septum, as well as other membrane-associated cytoskeletal structures such as the
383 septin ring (Wu et al., 2003), which may impact the force required for successful internalization.
384 Here, we demonstrate that endocytic patch behavior is intricately linked with cell polarization.
385 We find that endocytic patches at non-growing cell sides weakly recruit Fim1, display decreased
386 lifetimes, and exhibit diffusive behavior. In contrast, endocytic patches within polarized regions
387 recruit twice as much Fim1 with longer lifetimes, and exhibit directed motion during patch
388 internalization. While it is unclear if the endocytic patches at the cell sides successfully undergo
389 vesicle internalization. our data show that only the patches at the polarized sites exhibit the
390 controlled and directed motion required for orderly membrane invagination and vesicle scission.
391

392 **Cdc42 and Pak1 activity promote initiation of endocytosis at sites of polarization**

393 We show that Cdc42 activation is required for the initiation of branched actin-mediated
394 endocytosis at the division site. Similar to Cdc42 activation patterns, Fim1-mEGFP first appears
395 at the division site of *gef1*$^{+}$ controls during ring maturation well before the onset of ring
396 constriction (Wang et al., 2016). However, in *gef1Δ* mutants, Fim1-mEGFP appearance is
397 delayed to just before the onset of ring constriction, as reported for Cdc42 activation (Wei et al.,
398 2016). Yet, once Cdc42 is finally activated in *gef1Δ* mutants, Fim1-mEGFP rapidly appears at

399 the division site. These results suggest that the timing of Cdc42 activation and onset of
400 endocytosis are tightly linked. In a similar manner, we also demonstrate that the Cdc42
401 downstream effector Pak1 promotes timely onset of endocytosis at the division site. Given the
402 previously described challenges, we have not directly shown that Cdc42 activity is essential for
403 endocytosis at the cell ends. However, we demonstrate that decreased Cdc42 activation via
404 loss of its GEF *gef1* results in excessive Fim1 recruitment yet delayed patch internalization at
405 the cell ends. Thus, Gef1-mediated Cdc42 activation facilitates proper patch formation and
406 internalization at the cell ends.
407

408 **The two Cdc42 GEFs differentially regulate endocytosis**

409 As we probed how Cdc42 activation promotes endocytosis, we found that various polarity
410 mutants exhibit distinct phenotypes of endocytic patch behavior (summarized in Supplementary
411 Table S1, S2, and S3). Individual loss of each Cdc42 GEF results in disparate phenotypes. Loss
412 of *gef1* —where *scd1* is the sole Cdc42 GEF— severely impacts endocytic patch behavior at
413 polarized sites. On the other hand, loss of *scd1* —where *gef1* is the sole GEF— depolarizes the
414 location of endocytic sites across the cell cortex but the patch dynamics remain mostly normal.
415 These findings suggest that rather than strong, sustained activation via Scd1, transient, Gef1-
416 mediated Cdc42 activation is required for proper endocytic patch formation and internalization.
417 While dispensable for proper patch behavior, Scd1 is still required to prevent ectopic Cdc42
418 activation and thus regulates where endocytosis occurs. We observe that loss of *gef1* results in
419 some differences between patch dynamics at the cell ends and the division site. In *gef1*$^{+}$ cells,
420 peak Fim1-mEGFP patch intensity is reached ~2 seconds faster at the division site compared to
421 the cell ends. In contrast, *gef1Δ* mutants appear to recruit Fim1 to endocytic patches at both
422 sites with a delay. Additionally, Fim1-mEGFP patch lifetimes are increased at the cell ends of
423 *gef1Δ* mutants. Comparatively, patch lifetimes are not enhanced at the division site of *gef1Δ*

424 mutants, even though *gef1Δ* mutants recruit more Fim1 to endocytic patches. These
425 observations indicate that the rate of branched actin synthesis is likely faster in *gef1Δ* mutants,
426 since more branched actin is formed at the patch within the same span of time. As Cdc42 is
427 under strong Scd1-mediated activation in *gef1Δ* mutants, it is possible that sustained Cdc42
428 activity in these mutants leads to enhanced branched actin synthesis. Our results further show
429 that this excessive branched actin formation is actually deleterious to timely patch internalization
430 in *gef1Δ* mutants. Together, these findings indicate that Cdc42 activation must be tightly
431 regulated at the endocytic patch to form proper amounts of branched actin.
432
433 **Pak1 kinase differentially regulates endocytic patch dynamics at distinct sites**
434 Although loss of *pak1* kinase function impairs endocytic patch internalization at the cell ends
435 (Harrell et al., 2024), it seems that actin patch formation is most greatly impaired at the division
436 site of *pak1* mutants. At restrictive temperature, Fim1 recruitment to endocytic patches at the
437 cell ends is not impaired in *pak1* mutants, while it is greatly decreased at the division site. This
438 indicates that patch assembly at the cell ends is more robust to loss of *pak1* function than the
439 division site. However, as reported earlier, these patches do not internalize efficiently and often
440 fail endocytosis (Harrell et al., 2024). This suggests that Pak1 could play additional roles in
441 endocytosis apart from patch assembly. Alternatively, while the patch synthesizes sufficient
442 actin filaments, it may not be properly organized for successful internalization. We also see
443 enhanced patch assembly defects at the division site in *pak1* mutants. This suggests that Pak1
444 may play a more important role in at the division site that affects endocytosis. Already some
445 such roles are known since Pak1 phosphorylates several cytokinetic ring proteins (Magliozzi et
446 al., 2020) .
447
448 **Cdc42 and Pak1 kinase regulate Type I myosin recruitment and dynamics at sites of**
449 **endocytosis**

450 We show that Cdc42 promotes Myo1 recruitment to polarized sites in a dose-dependent
451 manner. Our data indicate that both insufficient and excessive Cdc42 activation leads to greater
452 stability of Myo1 at the plasma membrane, as demonstrated by its increased dwell time in
453 mutants of Cdc42 GEFs and GAPs and as well as the *pak1* kinase. This increased stability is
454 reminiscent of the stable localization displayed by Myo1-S361A-GFP, which cannot be
455 phosphorylated by Pak1 kinase at its motor domain TEDS site. Since endocytic patch
456 internalization defects seem to coincide with increased Myo1 stability, these results suggest that
457 Myo1 requires a certain level of dynamic behavior to properly promote endocytic patch
458 internalization. Since Myo1 is a direct target of Pak1 (Attanapola et al., 2009), we initially
459 expected *myo1-S361A* mutants to phenocopy the endocytic defects observed in kinase-dead
460 *pak1* mutants. Our results, however, show distinct phenotypes of altered endocytic patch
461 behavior for these mutants, which indicates that Pak1 has additional roles that are yet to be
462 explored.
463
464 In line with previous reports, our findings suggest that the Arp2/3 complex can generate
465 branched actin without Pak1 phosphorylation of Myo1's TEDS site (Attanapola et al., 2009) and
466 even without Myo1 altogether. Thus, the internalization defect observed in *myo1-S361A*
467 mutants does not stem from an inability to create branched actin. Given that TEDS site
468 phosphorylation promotes motor function of the Type I myosin in other organisms (Bement and
469 Mooseker, 1995; Fujita-Becker et al., 2005; Pedersen et al., 2023), we suspect that the same
470 likely occurs in *S. pombe*. Indeed, the perturbed localization and increased stability we observe
471 for Myo1-S361A-GFP suggests that its motor function may be impaired. Such findings have
472 been reported in budding yeast where Type I myosin motor activity is independent of its ability
473 to nucleate actin (Manenschijn et al., 2019). As the other actin nucleation promoting factor, the
474 WASP homolog Wsp1, activates Arp2/3 independently and more strongly than Myo1 in *S.*

475 *pombe* (Sirotkin et al., 2005), we suspect that Wsp1 primarily promotes Arp2/3-dependent
476 branched actin formation in *myo1-S361A* mutants.
477
478 Independent of Cdc42 and Pak1, Myo1 promotes patch assembly and dynamics at the cell
479 sides. In agreement, Pak1-dependent TEDS site phosphorylation of Myo1 does not appear to
480 be required at the cell sides. The patches at the cell sides contain less actin, have decreased
481 lifetimes, and do not rapidly internalization into the cell interior. It is possible that while Myo1
482 enables actin patch assembly at the cell sides, it may not generate sufficient branched actin
483 required for patch internalization. Sufficient branched actin assembly likely requires Pak1-
484 dependent phosphorylation of Myo1. This would explain why the patches at the polarized sites
485 show stronger internalization.
486
487 **Endocytic patch assembly and dynamics are differentially regulated at distinct cell sites**
488 While both the growing cell ends and the division site are sites of polarization, we observe
489 subtle differences in endocytic patch behavior between these sites. As endocytosis is a force-
490 sensitive and actin-dependent process, the differences in patch dynamics at these distinct sites
491 suggest that the forces experienced by patches at the division site are higher than that of the
492 cell ends. If such is the case, patches at the division site would require stronger actin
493 architecture and/or additional assistance from endocytic proteins such as Myo1 to overcome
494 this increased force. This disparate force requirement could arise in several ways. Perhaps the
495 flow of polarized secretion produces some counteractive force that must be overcome for
496 patches to internalize. At the division site, polarized secretion occurs throughout the division
497 plane, while endocytosis is largely confined to the outer rim of the membrane furrow (Wang et
498 al., 2016). Furthermore, our observations that endocytic patches at the cell sides are weakly
499 formed suggest that the forces they experience are also different than those at polarized
500 regions. It is unclear if the patches at the cell sides internalize, but do not move as far from the

501 plasma membrane since the force produced within the patch is less. It is possible that these
502 patches do not require access to active Cdc42 to internalize. Alternatively, it is possible that
503 they are random assemblies of branched actin that do not represent true sites of endocytosis.
504
505 Finally, it seems from our observations in *gef1Δ* mutants that formation of branched actin
506 patches is not sufficient in itself to stimulate timely patch internalization, since patches
507 excessively recruit both Cdc15 and Fim1 yet do not timely internalize. Perhaps the actin
508 architecture within these mutants is improperly organized to internalize the patch. This
509 hypothesis fits with our observations in *myo1Δ* and *myo1-S361A* mutants, which also assemble
510 branched actin patches with excessive Fim1 yet exhibit severe patch internalization defects.
511 Together, our findings indicate a direct role for Cdc42 in regulating endocytic patch formation via
512 the Pak1 kinase and endocytic patch internalization via the Pak1 target, the Type I myosin, in a
513 site-specific manner. A recent report characterized endocytic patch dynamics in different fungal
514 species including *S. pombe* (Picco et al., 2024). Compared to the other species, endocytic
515 patches in *S. pombe* appear to rapidly internalize at very high speeds deep into the cell interior
516 (Picco et al., 2024; Sun et al., 2019), which suggests the patches may experience higher
517 amounts of force which propel them inward at high velocity. Further investigation will determine
518 if Cdc42, Pak1 and Myo1 differentially regulate endocytosis in different fungal species resulting
519 in distinct dynamics.

520 **MATERIALS AND METHODS**

521 **Strains and cell culture**

522 The *S. pombe* strains used in this study are listed in Table 1. All strains are isogenic to the
523 original strain PN567. Cells were cultured in yeast extract (YE) medium and grown exponentially
524 at 25°C for 3 rounds of 8 generations before imaging. Standard techniques were used for
525 genetic manipulation and analysis (Moreno et al., 1991).
526

527 **Microscopy**

528 Imaging was performed at room temperature (23–25°C) for all experiments except for restrictive
529 temperature experiments, which were performed at 35°C (Fig. 5). Images were acquired on a
530 spinning disk confocal system equipped with a Nikon Eclipse inverted microscope with a
531 100×/1.49 NA lens, a CSU-22 spinning disk system (Yokogawa Electric Corporation), and a
532 Photometrics EM-CCD camera (Photometrics Technology Evolve with excelon Serial No:
533 A13B107000). On this system, images were acquired with MetaMorph (Molecular Devices,
534 Sunnyvale, CA). Imaging was also performed on a 3i spinning disk confocal system using a
535 Zeiss AxioObserver microscope equipped with a 100×/1.49 NA objective, an integrated
536 Yokogawa spinning disk (Yokogawa CSU-X1 A1 spinning disk scanner), and a Teledyne
537 Photometrics Prime 95b back-illuminated sCMOS camera (Serial No: A20D203014). On this
538 system, images were acquired using SlideBook (3i Intelligent Imaging innovations). All images
539 were analyzed with FIJI (National Institutes of Health, Bethesda, MD (Schneider et al., 2012)).
540

541 For still imaging, the cells were mounted directly on glass slides with a #1.5 coverslip (Thermo
542 Fisher Scientific, Waltham, MA) and imaged immediately, and with fresh slides prepared every
543 10 min. *Z*-series images were acquired with a depth interval of 0.4 μm. For time-lapse images,
544 cells were placed in 5 mm glass-bottom culture dishes (MatTek, Ashland, MA) and overlaid with

545 YE medium containing 0.6% agarose and 100 μM ascorbic acid as an antioxidant to minimize
546 toxicity to the cell, as reported previously (Frigault et al., 2009; Wei et al., 2017).
547
548 **Analysis of vesicle tracking**
549 Wild-type and mutant cells expressing Fim1-mEGFP or Fim1-mCherry were grown to OD 0.2-
550 0.5 and placed in glass-bottom culture dishes as previously described for time-lapse imaging.
551 Cells were imaged in a single medial plane with a frame rate of 1 sec for ~3-5 minutes using the
552 same laser power and exposure settings for all experiments. To measure patch lifetimes and
553 mean fluorescence intensity of patches throughout their lifetimes, Fim1-mEGFP/Fim1-mCherry
554 patches were tracked using the FIJI plugin TrackMate (Tinevez et al., 2017). Background
555 fluorescence was subtracted from the imaging field away from cells to sharpen the signal of
556 patches for ease of tracking. Lifetime was measured as the time from which a patch first
557 displayed distinguishable fluorescence at the cell cortex to when the fluorescence was no longer
558 detectable. Mean speed (μm/sec), MSD (mean squared displacement), and diffusion
559 coefficients (μm^2/sec) were all calculated using TrackMateR, an R package that can analyze
560 data captured and saved by TrackMate as XML files ((Sittewelle and Royle, 2024);
561 https://quantixed.org/2022/09/05/tracking-announcing-new-r-package-trackmater/). To ensure
562 that patches were tracked from the beginning of patch formation through patch disassembly,
563 patches selected for tracking 1. gradually increased in intensity until a peak intensity was
564 reached and 2. decreased in intensity following peak intensity (Berro and Pollard, 2014; Wang
565 et al., 2016). Patches tracked with TrackMate were also manually reviewed to ensure tracking
566 accuracy.

567 **Disruption of Pak1 kinase function via temperature-sensitive allele *orb2-34***

568 Pak1 kinase was inactivated via the *orb2-34* (*pak1-ts*) temperature-sensitive mutation. Cells
569 were grown for 2 days in YE medium. On the day of the experiment, cells were cultured to an

570 OD of 0.2. A subset of these cells was incubated at the permissive temperature of 25°C, while
571 the other set was incubated at the restrictive temperature of 35°C for 4 h. Cells were imaged
572 after 4 h under temperature-controlled conditions.

573 **Analysis of Myo1-GFP mean fluorescence intensity at cell ends**

574 Wild-type and mutant cells expressing Myo1-GFP were grown to OD 0.2-0.5 and imaged on
575 slides. Still *Z*-images with 21-24 *z*-planes were collected at a *z*-interval of 0.4 µm for the 488 nm
576 channel. The same number of *z*-slices were collected for wild-type and mutant cells for each
577 experiment using the same imaging settings. FIJI was used to generate sum projections from
578 the *z*-series and the polygon selection tool was used to encircle the "cap" of Myo1-GFP signal
579 present at individual cell ends. Mean fluorescence intensity at individual cell ends was then
580 measured within these manually selected Myo1-GFP "caps". The background fluorescence in a
581 cell-free region of the image was subtracted to normalize intensity measurements. Only cells
582 found within the central 80% of the imaging field were used for analysis. This was done to
583 account for uneven illumination of the imaging field.

584 **Analysis of Myo1-GFP dwell time at cell ends**

585 Wild-type and mutant cells expressing Myo1-GFP were grown to OD 0.2-0.5 and placed in
586 glass-bottom dishes as previously described for time-lapse imaging. Cells were imaged in a
587 single medial plane with a frame rate of 1 sec for 3 minutes using the same imaging settings for
588 all experiments. To visualize Myo1-GFP dwell time throughout the 3-minute time-lapse,
589 kymographs were generated from 1 pixel-wide selection lines drawn across the midline of the
590 cell end, parallel to the cell's long axis. These kymographs were then manually analyzed to
591 measure the dwell time of Myo1-GFP at individual cell ends in the following manner: Using
592 FIJI's rectangle selection tool, individual Myo1-GFP dwell time events were marked on each
593 kymograph and the length of each event was measured in pixels. Since our imaging settings

594 generated kymographs were 1 pixel = 1 sec, the number of pixels measured for an individual
595 event equals Myo1-GFP dwell time in seconds for that event.

596 **Statistical tests**

597 GraphPad Prism was used to determine significance. One-way ANOVA, followed by a Tukey's
598 multiple comparisons post-hoc test, was used to determine individual *p*-values when comparing
599 three or more samples. When comparing two samples, an unpaired Student's *t*-test (two-tailed,
600 unequal variance) was used to determine significance.

ACKNOWLEDGMENTS

We thank Drs. Vladimir Sirotkin and Daniel Mulvihill for strains; and Bret Judson for the Boston College imaging core facility.

COMPETING INTERESTS

No competing interests declared.

FUNDING

This research was supported by the National Science Foundation CAREER award #2309328 to MD.

AUTHOR CONTRIBUTIONS

M.E.D. and B.F.C. conceived the project. M.E.D. obtained funding for the project. B.F.C., A.R.W., and U.P. performed experiments and analyzed data. B.F.C. and M.E.D. wrote the manuscript.

DATA AND RESOURCE AVAILABILITY

Data and resource availability: All relevant data and resource can be found within the article and its supplementary information.

620 **REFERENCES**

621 **Adams, A. E., Johnson, D. I., Longnecker, R. M., Sloat, B. F. and Pringle, J. R.**
622 (1990). CDC42 and CDC43, two additional genes involved in budding and the establishment of
623 cell polarity in the yeast Saccharomyces cerevisiae. *J Cell Biol* **111**, 131-42.

624 **Aghamohammadzadeh, S. and Ayscough, K. R.** (2009). Differential requirements for
625 actin during yeast and mammalian endocytosis. *Nat Cell Biol* **11**, 1039-42.

626 **Arasada, R. and Pollard, T. D.** (2011). Distinct roles for F-BAR proteins Cdc15p and
627 Bzz1p in actin polymerization at sites of endocytosis in fission yeast. *Curr Biol* **21**, 1450-9.

628 **Attanapola, S. L., Alexander, C. J. and Mulvihill, D. P.** (2009). Ste20-kinase-
629 dependent TEDS-site phosphorylation modulates the dynamic localisation and endocytic
630 function of the fission yeast class I myosin, Myo1. *J Cell Sci* **122**, 3856-61.

631 **Basu, R., Munteanu, E. L. and Chang, F.** (2014). Role of turgor pressure in
632 endocytosis in fission yeast. *Mol Biol Cell* **25**, 679-87.

633 **Bement, W. M. and Mooseker, M. S.** (1995). TEDS rule: a molecular rationale for
634 differential regulation of myosins by phosphorylation of the heavy chain head. *Cell Motil*
635 *Cytoskeleton* **31**, 87-92.

636 **Berro, J. and Pollard, T. D.** (2014). Local and global analysis of endocytic patch
637 dynamics in fission yeast using a new "temporal superresolution" realignment method. *Mol Biol*
638 *Cell* **25**, 3501-14.

639 **Bokoch, G. M.** (2003). Biology of the p21-activated kinases. *Annu Rev Biochem* **72**,
640 743-81.

641 **Brzeska, H., Knaus, U. G., Wang, Z. Y., Bokoch, G. M. and Korn, E. D.** (1997). p21-
642 activated kinase has substrate specificity similar to Acanthamoeba myosin I heavy chain kinase
643 and activates Acanthamoeba myosin I. *Proc Natl Acad Sci U S A* **94**, 1092-5.

644 **Campbell, B. F., Hercyk, B. S., Williams, A. R., San Miguel, E., Young, H. G. and**
645 **Das, M. E.** (2022). Cdc42 GTPase activating proteins Rga4 and Rga6 coordinate septum
646 synthesis and membrane trafficking at the division plane during cytokinesis. *Traffic* **23**, 478-495.
647 **Carnahan, R. H. and Gould, K. L.** (2003). The PCH family protein, Cdc15p, recruits two
648 F-actin nucleation pathways to coordinate cytokinetic actin ring formation in
649 Schizosaccharomyces pombe. *J Cell Biol* **162**, 851-62.
650 **Coll, P. M., Trillo, Y., Ametzazurra, A. and Perez, P.** (2003). Gef1p, a new guanine
651 nucleotide exchange factor for Cdc42p, regulates polarity in Schizosaccharomyces pombe. *Mol*
652 *Biol Cell* **14**, 313-23.
653 **Das, M., Drake, T., Wiley, D. J., Buchwald, P., Vavylonis, D. and Verde, F.** (2012).
654 Oscillatory dynamics of Cdc42 GTPase in the control of polarized growth. *Science* **337**, 239-43.
655 **Das, M., Nuñez, I., Rodriguez, M., Wiley, D. J., Rodriguez, J., Sarkeshik, A., Yates,**
656 **J. R., 3rd, Buchwald, P. and Verde, F.** (2015). Phosphorylation-dependent inhibition of Cdc42
657 GEF Gef1 by 14-3-3 protein Rad24 spatially regulates Cdc42 GTPase activity and oscillatory
658 dynamics during cell morphogenesis. *Mol Biol Cell* **26**, 3520-34.
659 **Das, M. and Verde, F.** (2013). Role of Cdc42 dynamics in the control of fission yeast
660 cell polarization. *Biochem Soc Trans* **41**, 1745-9.
661 **Frigault, M. M., Lacoste, J., Swift, J. L. and Brown, C. M.** (2009). Live-cell microscopy
662 - tips and tools. *J Cell Sci* **122**, 753-67.
663 **Fujita-Becker, S., Dürrwang, U., Erent, M., Clark, R. J., Geeves, M. A. and Manstein,**
664 **D. J.** (2005). Changes in Mg2+ ion concentration and heavy chain phosphorylation regulate the
665 motor activity of a class I myosin. *J Biol Chem* **280**, 6064-71.
666 **Gachet, Y. and Hyams, J. S.** (2005). Endocytosis in fission yeast is spatially associated
667 with the actin cytoskeleton during polarised cell growth and cytokinesis. *J Cell Sci* **118**, 4231-42.

668 **Harrell, M. A., Liu, Z., Campbell, B. F., Chinsen, O., Hong, T. and Das, M.** (2024).
669 Arp2/3-dependent endocytosis ensures Cdc42 oscillations by removing Pak1-mediated negative
670 feedback. *J Cell Biol* **223**.
671 **Hercyk, B. and Das, M.** (2019a). Rho Family GTPases in Fission Yeast Cytokinesis.
672 *Commun Integr Biol* **12**, 171-180.
673 **Hercyk, B. S. and Das, M. E.** (2019b). F-BAR Cdc15 Promotes Cdc42 Activation During
674 Cytokinesis and Cell Polarization in Schizosaccharomyces pombe. *Genetics* **213**, 1341-1356.
675 **Hercyk, B. S., Rich-Robinson, J., Mitoubsi, A. S., Harrell, M. A. and Das, M. E.**
676 (2019). A novel interplay between GEFs orchestrates Cdc42 activity during cell polarity and
677 cytokinesis in fission yeast. *J Cell Sci* **132**.
678 **Kaksonen, M. and Roux, A.** (2018). Mechanisms of clathrin-mediated endocytosis. *Nat*
679 *Rev Mol Cell Biol* **19**, 313-326.
680 **Kroschewski, R., Hall, A. and Mellman, I.** (1999). Cdc42 controls secretory and
681 endocytic transport to the basolateral plasma membrane of MDCK cells. *Nat Cell Biol* **1**, 8-13.
682 **Lacy, M. M., Ma, R., Ravindra, N. G. and Berro, J.** (2018). Molecular mechanisms of
683 force production in clathrin-mediated endocytosis. *FEBS Lett* **592**, 3586-3605.
684 **Lamas, I., Merlini, L., Vještica, A., Vincenzetti, V. and Martin, S. G.** (2020).
685 Optogenetics reveals Cdc42 local activation by scaffold-mediated positive feedback and Ras
686 GTPase. *PLoS Biol* **18**, e3000600.
687 **Lechler, T., Jonsdottir, G. A., Klee, S. K., Pellman, D. and Li, R.** (2001). A two-tiered
688 mechanism by which Cdc42 controls the localization and activation of an Arp2/3-activating
689 motor complex in yeast. *J Cell Biol* **155**, 261-70.
690 **Lechler, T., Shevchenko, A. and Li, R.** (2000). Direct involvement of yeast type I
691 myosins in Cdc42-dependent actin polymerization. *J Cell Biol* **148**, 363-73.

692 **Lee, W. L., Bezanilla, M. and Pollard, T. D.** (2000). Fission yeast myosin-I, Myo1p,
693 stimulates actin assembly by Arp2/3 complex and shares functions with WASp. *J Cell Biol* **151**,
694 789-800.
695 **Magliozzi, J. O., Sears, J., Cressey, L., Brady, M., Opalko, H. E., Kettenbach, A. N.**
696 **and Moseley, J. B.** (2020). Fission yeast Pak1 phosphorylates anillin-like Mid1 for spatial
697 control of cytokinesis. *J Cell Biol* **219**.
698 **Manenschijn, H. E., Picco, A., Mund, M., Rivier-Cordey, A. S., Ries, J. and**
699 **Kaksonen, M.** (2019). Type-I myosins promote actin polymerization to drive membrane bending
700 in endocytosis. *Elife* **8**.
701 **Manser, E., Leung, T., Salihuddin, H., Zhao, Z. S. and Lim, L.** (1994). A brain
702 serine/threonine protein kinase activated by Cdc42 and Rac1. *Nature* **367**, 40-6.
703 **Marcus, S., Polverino, A., Chang, E., Robbins, D., Cobb, M. H. and Wigler, M. H.**
704 (1995). Shk1, a homolog of the Saccharomyces cerevisiae Ste20 and mammalian p65PAK
705 protein kinases, is a component of a Ras/Cdc42 signaling module in the fission yeast
706 Schizosaccharomyces pombe. *Proc Natl Acad Sci U S A* **92**, 6180-4.
707 **Moreno, S., Klar, A. and Nurse, P.** (1991). Molecular genetic analysis of fission yeast
708 Schizosaccharomyces pombe. *Methods Enzymol* **194**, 795-823.
709 **Murray, J. M. and Johnson, D. I.** (2001). The Cdc42p GTPase and its regulators Nrf1p
710 and Scd1p are involved in endocytic trafficking in the fission yeast Schizosaccharomyces
711 pombe. *J Biol Chem* **276**, 3004-9.
712 **Nakano, K., Satoh, K., Morimatsu, A., Ohnuma, M. and Mabuchi, I.** (2001).
713 Interactions among a fimbrin, a capping protein, and an actin-depolymerizing factor in
714 organization of the fission yeast actin cytoskeleton. *Mol Biol Cell* **12**, 3515-26.
715 **Nickaeen, M., Berro, J., Pollard, T. D. and Slepchenko, B. M.** (2022). A model of
716 actin-driven endocytosis explains differences of endocytic motility in budding and fission yeast.
717 *Mol Biol Cell* **33**, ar16.

718 **Onwubiko, U. N., Mlynarczyk, P. J., Wei, B., Habiyaremye, J., Clack, A., Abel, S. M.**
719 **and Das, M. E.** (2019). A Cdc42 GEF, Gef1, through endocytosis organizes F-BAR Cdc15
720 along the actomyosin ring and promotes concentric furrowing. *J Cell Sci* **132**.
721 **Ottilie, S., Miller, P. J., Johnson, D. I., Creasy, C. L., Sells, M. A., Bagrodia, S.,**
722 **Forsburg, S. L. and Chernoff, J.** (1995). Fission yeast pak1+ encodes a protein kinase that
723 interacts with Cdc42p and is involved in the control of cell polarity and mating. *Embo j* **14**, 5908-
724 19.
725 **Pedersen, R. T. A., Snoberger, A., Pyrpassopoulos, S., Safer, D., Drubin, D. G. and**
726 **Ostap, E. M.** (2023). Endocytic myosin-1 is a force-insensitive, power-generating motor. *J Cell*
727 *Biol* **222**.
728 **Picco, A., Toret, C. P., Rivier-Cordey, A.-S. and Kaksonen, M.** (2024). An
729 evolutionary cell biology perspective into the diverging mechanisms of clathrin-mediated
730 endocytosis in dikarya fungi. *bioRxiv*, 2024.03.28.587219.
731 **Schneider, C. A., Rasband, W. S. and Eliceiri, K. W.** (2012). NIH Image to ImageJ: 25
732 years of image analysis. *Nat Methods* **9**, 671-5.
733 **Sirotkin, V., Beltzner, C. C., Marchand, J. B. and Pollard, T. D.** (2005). Interactions of
734 WASp, myosin-I, and verprolin with Arp2/3 complex during actin patch assembly in fission
735 yeast. *J Cell Biol* **170**, 637-48.
736 **Sirotkin, V., Berro, J., Macmillan, K., Zhao, L. and Pollard, T. D.** (2010). Quantitative
737 analysis of the mechanism of endocytic actin patch assembly and disassembly in fission yeast.
738 *Mol Biol Cell* **21**, 2894-904.
739 **Sittewelle, M. and Royle, S. J.** (2024). Passive diffusion accounts for the majority of
740 intracellular nanovesicle transport. *Life Sci Alliance* **7**.
741 **Skau, C. T., Courson, D. S., Bestul, A. J., Winkelman, J. D., Rock, R. S., Sirotkin, V.**
742 **and Kovar, D. R.** (2011). Actin filament bundling by fimbrin is important for endocytosis,
743 cytokinesis, and polarization in fission yeast. *J Biol Chem* **286**, 26964-77.

744 **Sun, Y., Schoneberg, J., Chen, X., Jiang, T., Kaplan, C., Xu, K., Pollard, T. D. and**
745 **Drubin, D. G.** (2019). Direct comparison of clathrin-mediated endocytosis in budding and fission
746 yeast reveals conserved and evolvable features. *Elife* **8**.
747 **Tatebe, H., Nakano, K., Maximo, R. and Shiozaki, K.** (2008). Pom1 DYRK regulates
748 localization of the Rga4 GAP to ensure bipolar activation of Cdc42 in fission yeast. *Curr Biol* **18**,
749 322-30.
750 **Tinevez, J. Y., Perry, N., Schindelin, J., Hoopes, G. M., Reynolds, G. D., Laplantine,**
751 **E., Bednarek, S. Y., Shorte, S. L. and Eliceiri, K. W.** (2017). TrackMate: An open and
752 extensible platform for single-particle tracking. *Methods* **115**, 80-90.
753 **Verde, F., Mata, J. and Nurse, P.** (1995). Fission yeast cell morphogenesis:
754 identification of new genes and analysis of their role during the cell cycle. *J Cell Biol* **131**, 1529-
755 38.
756 **Wang, N., Lee, I. J., Rask, G. and Wu, J. Q.** (2016). Roles of the TRAPP-II Complex
757 and the Exocyst in Membrane Deposition during Fission Yeast Cytokinesis. *PLoS Biol* **14**,
758 e1002437.
759 **Wei, B., Hercyk, B. S., Habiyaremye, J. and Das, M.** (2017). Spatiotemporal Analysis
760 of Cytokinetic Events in Fission Yeast. *J Vis Exp*.
761 **Wei, B., Hercyk, B. S., Mattson, N., Mohammadi, A., Rich, J., DeBruyne, E., Clark,**
762 **M. M. and Das, M.** (2016). Unique spatiotemporal activation pattern of Cdc42 by Gef1 and Scd1
763 promotes different events during cytokinesis. *Mol Biol Cell* **27**, 1235-45.
764 **Wu, C., Lytvyn, V., Thomas, D. Y. and Leberer, E.** (1997). The phosphorylation site for
765 Ste20p-like protein kinases is essential for the function of myosin-I in yeast. *J Biol Chem* **272**,
766 30623-6.
767 **Wu, J. Q., Kuhn, J. R., Kovar, D. R. and Pollard, T. D.** (2003). Spatial and temporal
768 pathway for assembly and constriction of the contractile ring in fission yeast cytokinesis. *Dev*
769 *Cell* **5**, 723-34.

770 **FIGURE LEGENDS**

771 **Figure. 1**. **Endocytic events at distinct sites in the cell show differential dynamics.**
772 **A.** Endocytic events occur at different regions of polarized *S. pombe* cells. Colored tracks
773 indicate trajectories of individual Fim1-mEGFP patches. **B.** Lifetimes of Fim1-mEGFP
774 labeled endocytic patches at each region. **C.** Mean Fim1-mEGFP peak intensity in
775 endocytic patches at each region. **D.** Mean speed of endocytic patches at each region
776 averaged from individual cells. **E.** MSD (mean square displacement) of Fim1-mEGFP
777 patches calculated for each region. **F.** Diffusion coefficient of Fim1-mEGFP patches at
778 each region. (n ≥ 28 patches per region, N=3; n ≥ 6 cells analyzed per region). Ordinary
779 one-way ANOVA with Tukey's multiple comparisons. ****, $p < 0.0001$; **, $p < 0.01$

780

781 **Figure 2. Endocytosis follows Cdc42 activation at the division site.**
782 **A.** Representative cells showing initial (green dotted box) and uniform (solid green box)
783 Fim1-mEGFP appearance at the division site relative to Sad1-mCherry labeled spindle
784 pole body (SPB) separation (purple arrowhead). **B.** Quantification of A, where time 0 =
785 SPB separation. **C.** Representative cells showing initial (purple dotted box) and uniform
786 (solid purple box) Fim1-mCherry appearance relative to CRIB-3xGFP appearance (green
787 box) at the division site. **D.** Quantification of C, where time 0 marks CRIB-3xGFP
788 appearance (green arrowheads) at the division site. (n ≥ 8 cells per genotype per
789 experiment). Unpaired Student's *t*-test. ****, $p < 0.0001$; ***, $p < 0.001$; **, $p < 0.01$, scale
790 bar=5μm

791

792 **Figure 3. The Cdc42 GEFs Gef1 and Scd1 differentially regulate endocytosis.**

793 **A.** Representative montages of Cdc15-tdTom and Fim1-mEGFP at growing cell ends in
794 the indicated genotypes. **B-G.** Mean patch intensities of Fim1-mEGFP at growing cell
795 ends, the division site, and cell sides. (n ≥ 20 endocytic patches per triplicate experiment).
796 **H.** and **I.** Patch lifetimes of Fim1-mEGFP at each region in the indicated genotypes. (n ≥
797 20 endocytic patches, N=3). Ordinary one-way ANOVA with Tukey's multiple
798 comparisons. ****, $p<0.0001$; ***, $p<0.001$; **, $p<0.01$; *, $p< 0.05$; ns, not significant
799
800 **Figure 4. Pak1/Orb2 kinase is required for timely initiation of endocytosis at the**
801 **division site. A.** Representative *orb2+* and *orb2-34* cells showing initial (green dotted
802 box) and uniform (solid green box) Fim1-mEGFP appearance at the division site relative
803 to Sad1-mCherry to mark spindle pole body separation (purple arrowhead. **B-C.**
804 Quantification of A, where time 0 = SPB separation. (n ≥ 8 cells per genotype per
805 experiment). Unpaired Student's *t*-test. **, $p<0.01$; *, $p< 0.05$, scale bar=5μm
806
807 **Figure 5. Pak1/Orb2 kinase is required for normal endocytic patch dynamics at the**
808 **cell ends.**
809 **A.** Representative cells showing Fim1-mEGFP endocytic events tracked via TrackMate.
810 **B-G.** Mean patch intensities of Fim1-mEGFP at growing cell ends, the division site, and
811 cell sides in the indicated genotypes and conditions. (n ≥ 20 endocytic patches per
812 experiment). **H-I.** Patch lifetimes of Fim1-mEGFP at each region in the indicated
813 genotypes and conditions. (n ≥ 20 endocytic patches, N=3). Ordinary one-way ANOVA
814 with Tukey's multiple comparisons. ****, $p<0.0001$; ***, $p<0.001$; **, $p<0.01$; *, $p< 0.05$;
815 ns, not significant

816 **Figure 6. The type 1 Myosin Myo1 regulates endocytic patch dynamics at the cell**
817 **ends, division site and the cell sides.**
818 **A.** Representative cells showing Fim1-mCherry endocytic events tracked via TrackMate
819 in the indicated strains. **B.** Patch lifetimes of Fim1-mCherry at each region in *myo1*$^{+}$ and
820 *myo1Δ*. **C**. Patch lifetimes of Fim1-mCherry at each region in *myo1*$^{+}$ and *myo1S361A*. **D.**
821 Montages of Fim1-mCherry overtime at the cell ends of the indicated strains. **E-J.** Mean
822 patch intensities of Fim1-mCherry at each region of the indicated strains. (n ≥ 17
823 endocytic patches, N=3). Ordinary one-way ANOVA with Tukey's multiple comparisons.
824 ****, p<0.0001; ***, p<0.001; **, p<0.01; *, p< 0.05; ns, not significant
825
826 **Figure 7. Myo1 localization to the division site requires Cdc42 and Pak1/Orb2**
827 **kinase.**
828 **A** and **D.** Representative cells showing Myo1-GFP appearance (green box) at the division
829 site relative to Sad1-mCherry to mark spindle pole body (SPB) separation (purple
830 arrowhead) in the indicated strains. **B** and **C.** Quantification of A and D, respectively,
831 where time 0 = SPB separation. (n ≥ 10 cells per genotype per experiment). Unpaired
832 Student's *t*-test. ***, p<0.001; **, p<0.01, scale bar=5μm
833
834 **Figure 8. Cdc42 and Pak1/Orb2 kinase promotes Myo1 localization to the cell ends**
835 **and division site.**
836 **A** and **E.** Sum Z-projections of Myo1-GFP in the indicated strains and conditions. **B** and
837 **F.** Mean Myo1-GFP intensity measured at cell ends in the indicated strains (n=15 cells
838 per genotype per triplicate experiment). **C** and **G.** Quantification of dwell times of Myo1-

839 GFP in indicated strains. (n≥15 dwell time events per genotype. **D** and **H.** Montages
840 showing Myo1-GFP dwell time dynamics at individual cell ends. One-way ANOVA with
841 Tukey's multiple comparisons post hoc test. ns, not significant; *, $p<0.05$; **, p.<0.01; ***,
842 $p<0.001$; ****, p<0.0001, scale bar=5μm

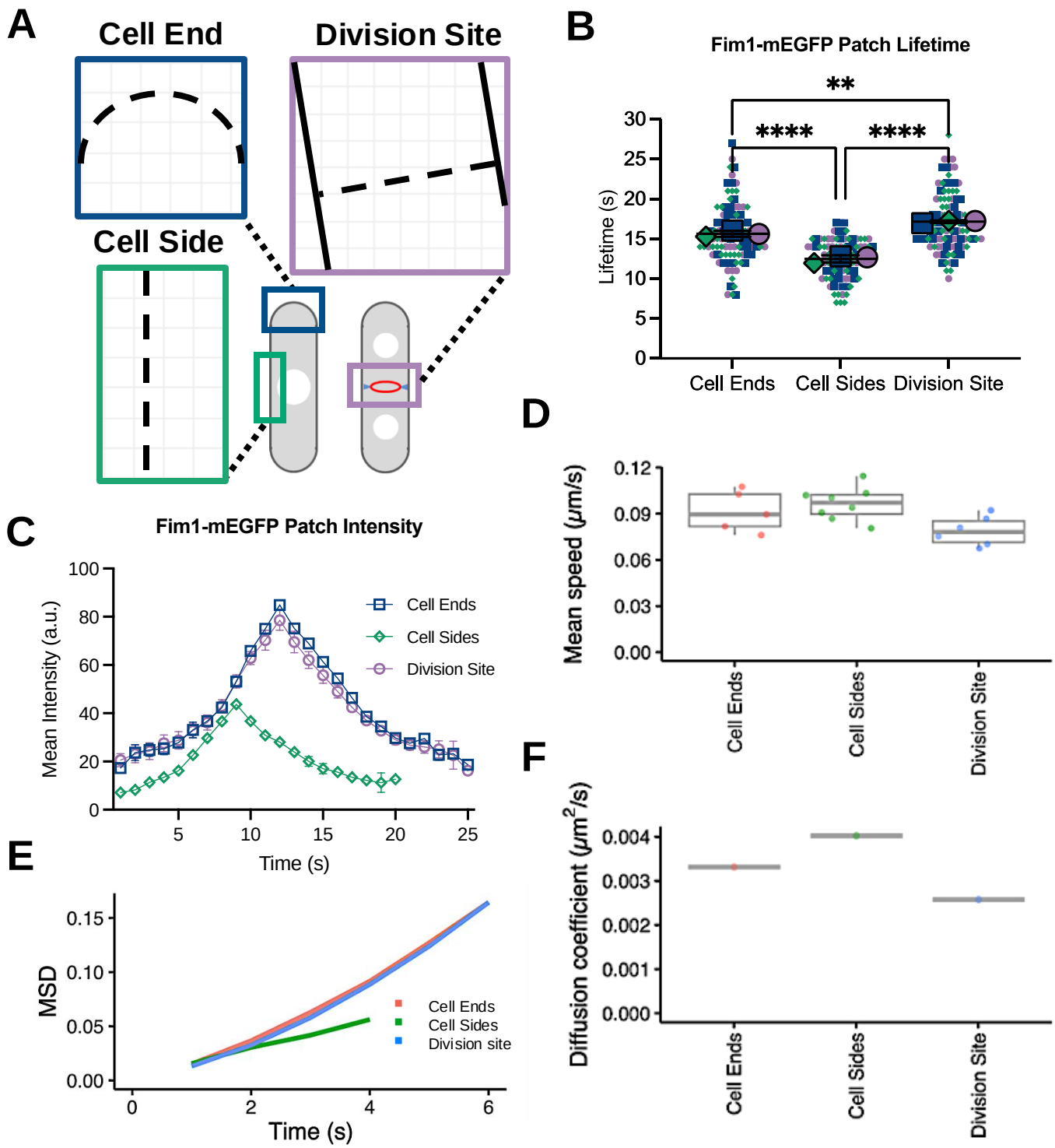
A
Cell End
Division Site
Cell Side
B
Fim1-mEGFP Patch Lifetime
**
****
****
Lifetime (s)
30
25
20
15
10
5
0
Cell Ends
Cell Sides
Division Site
C
Fim1-mEGFP Patch Intensity
Mean Intensity (a.u.)
100
80
60
40
20
0
5
10
15
20
25
Time (s)
Cell Ends
Cell Sides
Division Site
D
Mean speed (μm/s)
0.12
0.09
0.06
0.03
0.00
Cell Ends
Cell Sides
Division Site
E
MSD
0.15
0.10
0.05
0.00
0
2
4
6
Time (s)
Cell Ends
Cell Sides
Division site
F
Diffusion coefficient (μm²/s)
0.004
0.003
0.002
0.001
0.000
Cell Ends
Cell Sides
Division Site

Figure 1

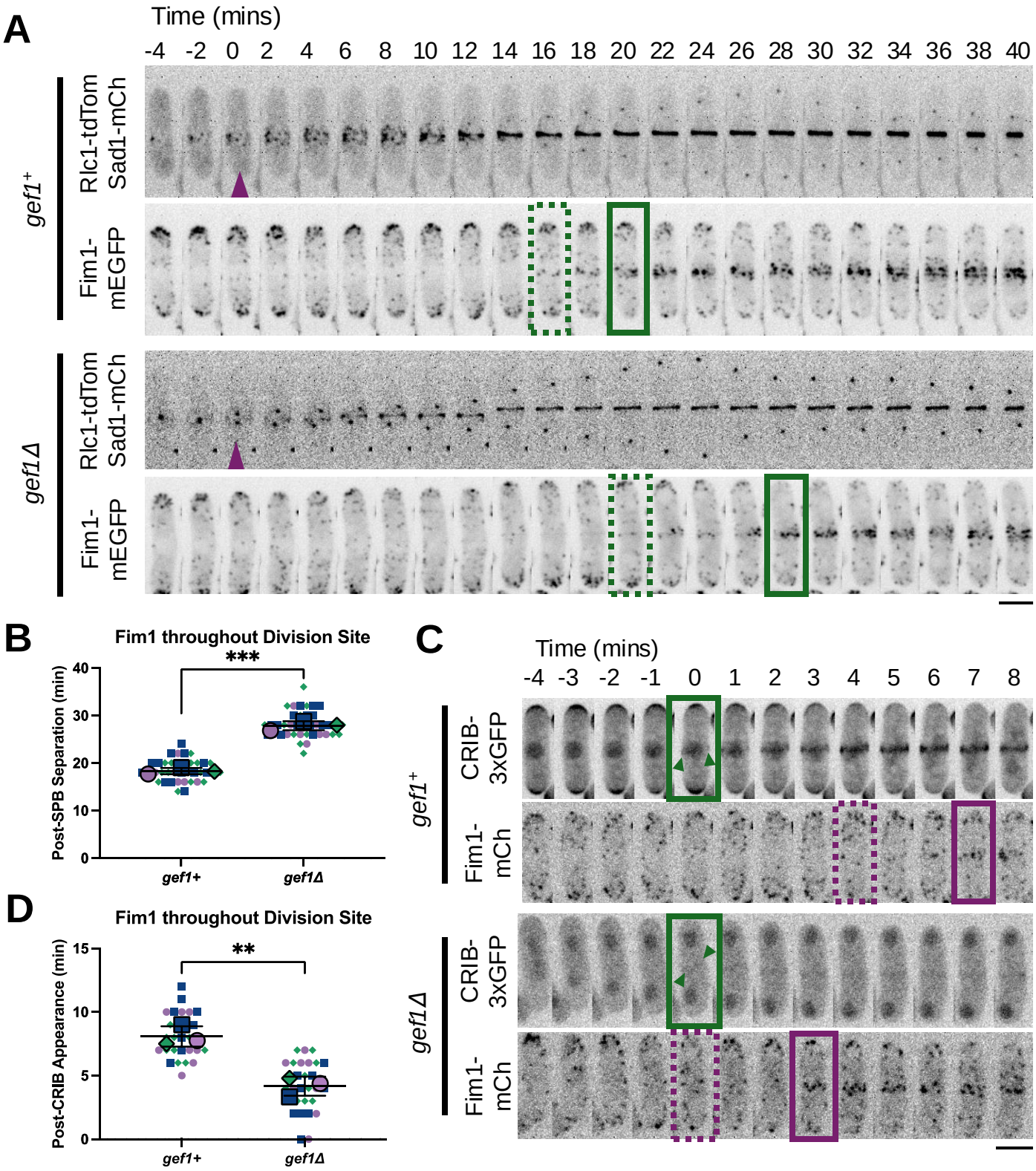
A
Time (mins)
-4 -2 0 2 4 6 8 10 12 14 16 18 20 22 24 26 28 30 32 34 36 38 40
gef1+
Rlc1-tdTom
Sad1-mCh
Fim1-
mEGFP
gef1Δ
Rlc1-tdTom
Sad1-mCh
Fim1-
mEGFP
B
Fim1 throughout Division Site
***
Post-SPB Separation (min)
0
10
20
30
40
gef1+
gef1Δ
C
Time (mins)
-4 -3 -2 -1 0 1 2 3 4 5 6 7 8
gef1+
CRIB-
3xGFP
Fim1-
mCh
gef1Δ
CRIB-
3xGFP
Fim1-
mCh
D
Fim1 throughout Division Site
**
Post-CRIB Appearance (min)
0
5
10
15
gef1+
gef1Δ

Figure 2

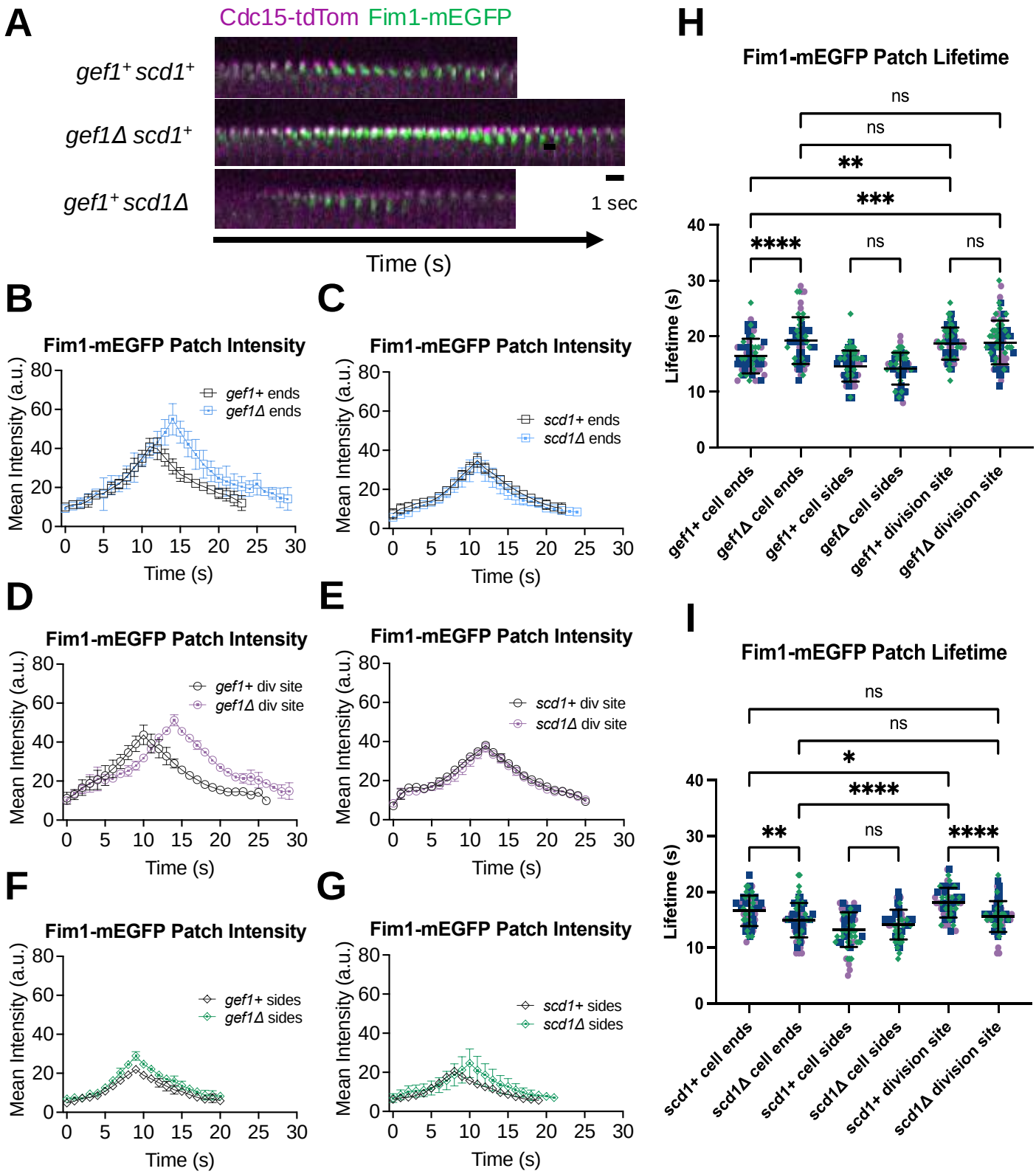
A
Cdc15-tdTom Fim1-mEGFP
gef1⁺ scd1⁺
gef1Δ scd1⁺
gef1⁺ scd1Δ
1 sec
Time (s)
B
Fim1-mEGFP Patch Intensity
Mean Intensity (a.u.)
gef1+ ends
gef1Δ ends
Time (s)
C
Fim1-mEGFP Patch Intensity
Mean Intensity (a.u.)
scd1+ ends
scd1Δ ends
Time (s)
D
Fim1-mEGFP Patch Intensity
Mean Intensity (a.u.)
gef1+ div site
gef1Δ div site
Time (s)
E
Fim1-mEGFP Patch Intensity
Mean Intensity (a.u.)
scd1+ div site
scd1Δ div site
Time (s)
F
Fim1-mEGFP Patch Intensity
Mean Intensity (a.u.)
gef1+ sides
gef1Δ sides
Time (s)
G
Fim1-mEGFP Patch Intensity
Mean Intensity (a.u.)
scd1+ sides
scd1Δ sides
Time (s)
H
Fim1-mEGFP Patch Lifetime
Lifetime (s)
ns
ns
**
***
****
ns
ns
gef1+ cell ends
gef1Δ cell ends
gef1+ cell sides
gefΔ cell sides
gef1+ division site
gef1Δ division site
I
Fim1-mEGFP Patch Lifetime
Lifetime (s)
ns
ns
*
****
**
ns
****
scd1+ cell ends
scd1Δ cell ends
scd1+ cell sides
scd1Δ cell sides
scd1+ division site
scd1Δ division site

Figure 3

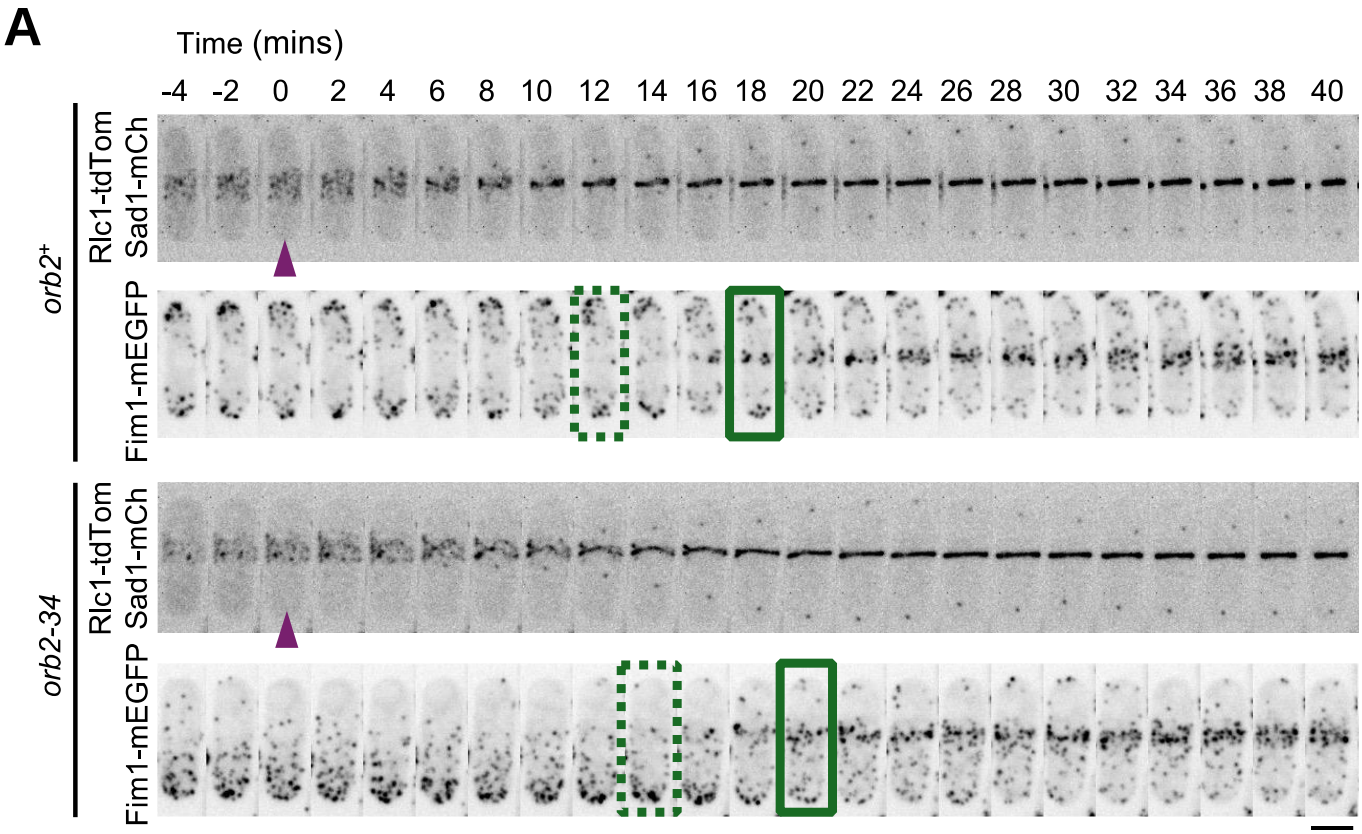
A
Time (mins)
-4 -2 0 2 4 6 8 10 12 14 16 18 20 22 24 26 28 30 32 34 36 38 40
orb2+
Rlc1-tdTom
Sad1-mCh
Fim1-mEGFP
orb2-34
Rlc1-tdTom
Sad1-mCh
Fim1-mEGFP

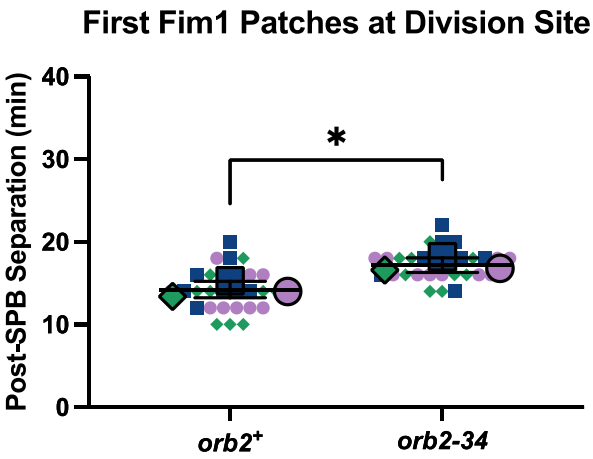
B
First Fim1 Patches at Division Site
Post-SPB Separation (min)
0
10
20
30
40
*
orb2+
orb2-34

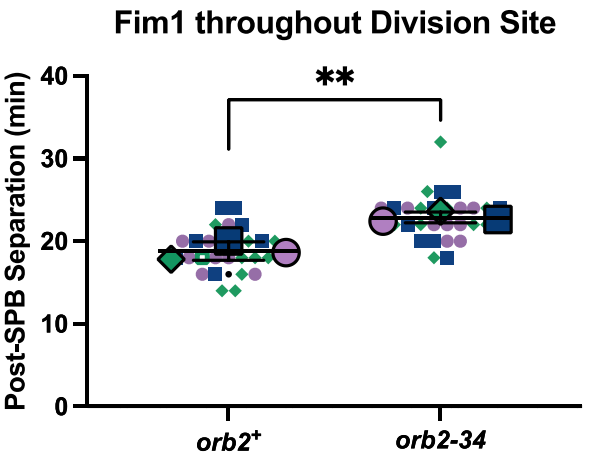
C
Fim1 throughout Division Site
Post-SPB Separation (min)
0
10
20
30
40
**
orb2+
orb2-34

Figure 4

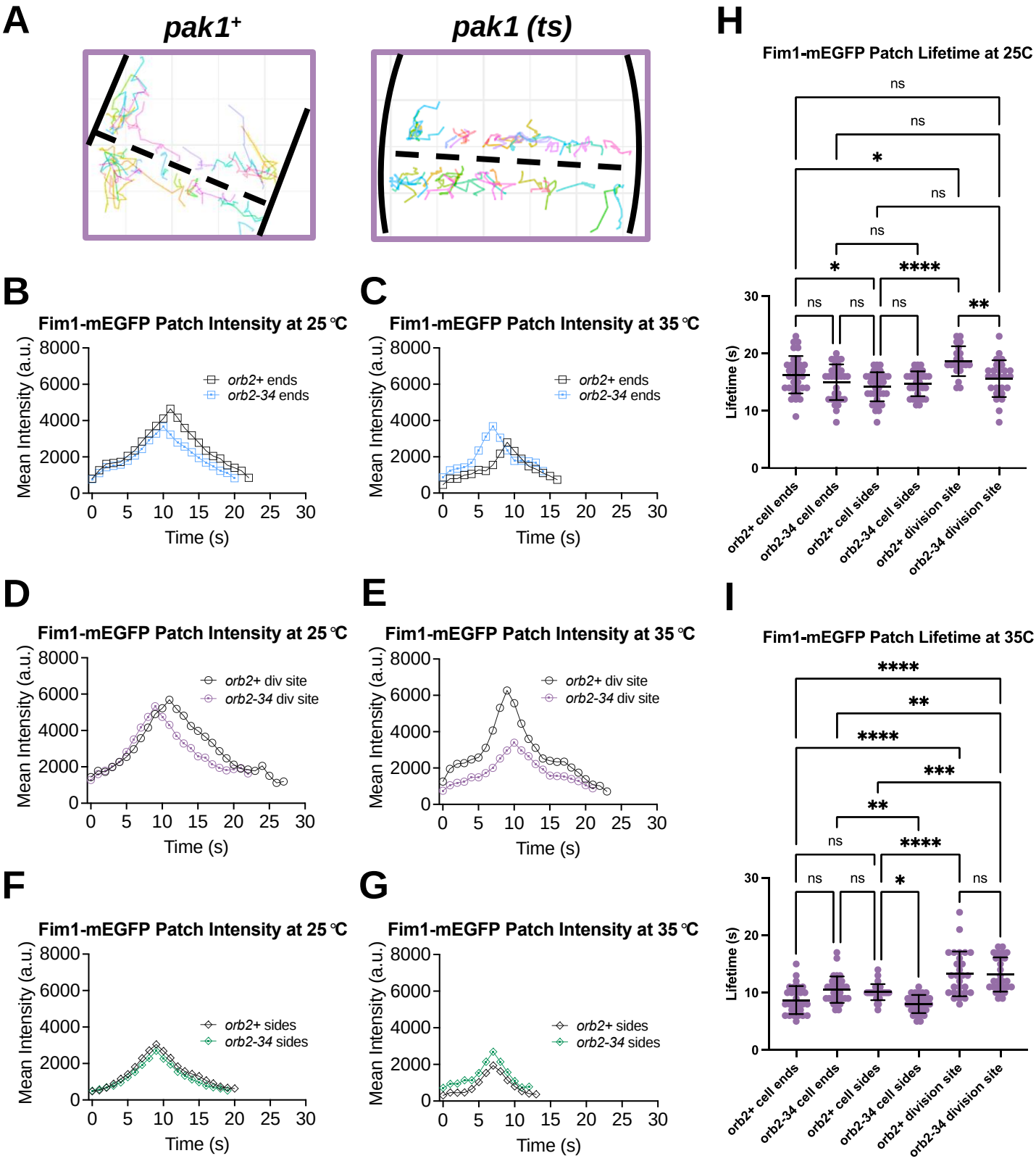
A
pak1+
pak1 (ts)
B
Fim1-mEGFP Patch Intensity at 25 ℃
Mean Intensity (a.u.)
Time (s)
orb2+ ends
orb2-34 ends
C
Fim1-mEGFP Patch Intensity at 35 ℃
D
Fim1-mEGFP Patch Intensity at 25 ℃
orb2+ div site
orb2-34 div site
E
Fim1-mEGFP Patch Intensity at 35 ℃
F
Fim1-mEGFP Patch Intensity at 25 ℃
orb2+ sides
orb2-34 sides
G
Fim1-mEGFP Patch Intensity at 35 ℃
H
Fim1-mEGFP Patch Lifetime at 25C
Lifetime (s)
orb2+ cell ends
orb2-34 cell ends
orb2+ cell sides
orb2-34 cell sides
orb2+ division site
orb2-34 division site
I
Fim1-mEGFP Patch Lifetime at 35C

Figure 5

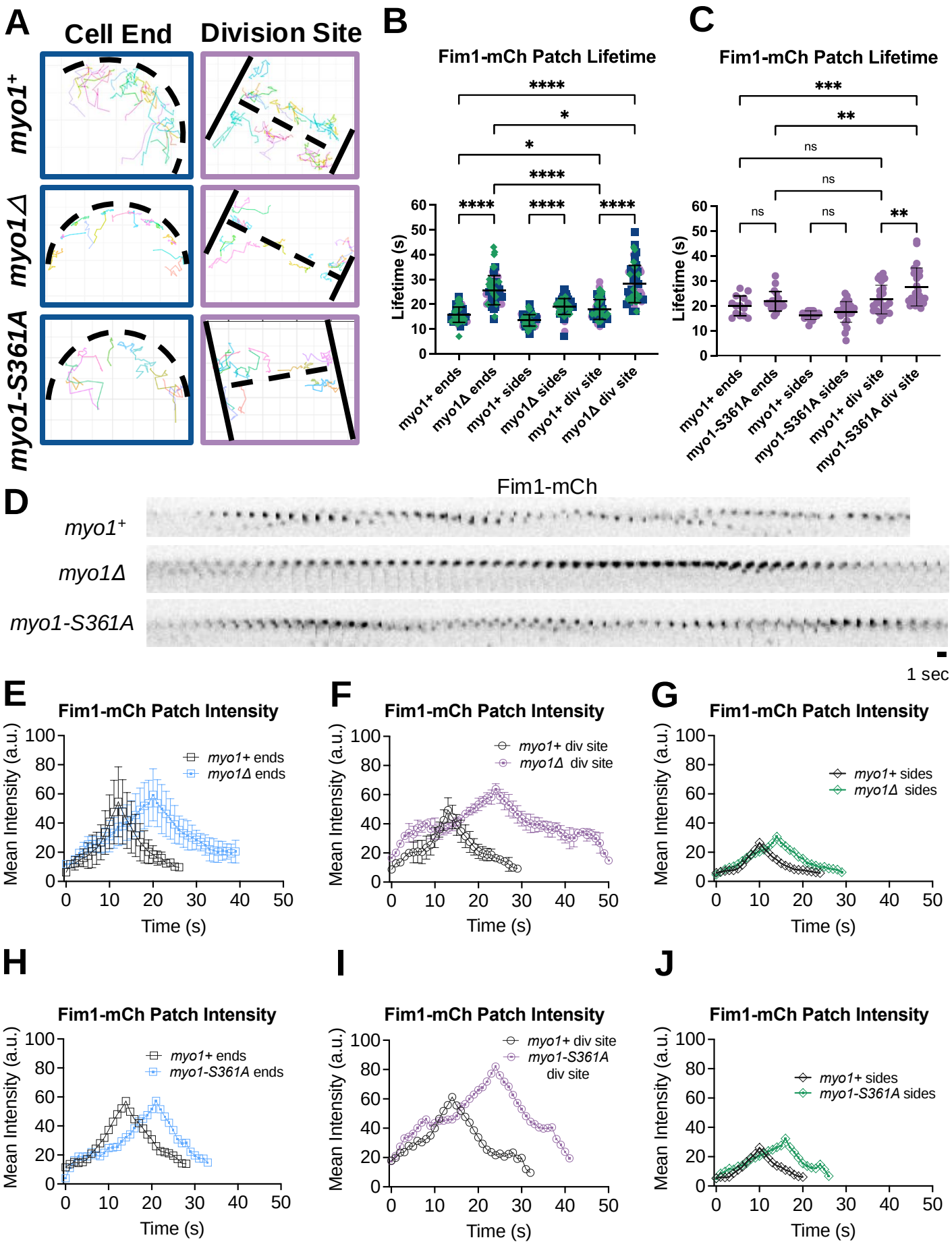
A
Cell End
Division Site
myo1+
myo1Δ
myo1-S361A
B
Fim1-mCh Patch Lifetime
Lifetime (s)
myo1+ ends
myo1Δ ends
myo1+ sides
myo1Δ sides
myo1+ div site
myo1Δ div site
C
Fim1-mCh Patch Lifetime
Lifetime (s)
myo1+ ends
myo1-S361A ends
myo1+ sides
myo1-S361A sides
myo1+ div site
myo1-S361A div site
D
Fim1-mCh
myo1+
myo1Δ
myo1-S361A
1 sec
E
Fim1-mCh Patch Intensity
Mean Intensity (a.u.)
Time (s)
myo1+ ends
myo1Δ ends
F
Fim1-mCh Patch Intensity
Mean Intensity (a.u.)
Time (s)
myo1+ div site
myo1Δ div site
G
Fim1-mCh Patch Intensity
Mean Intensity (a.u.)
Time (s)
myo1+ sides
myo1Δ sides
H
Fim1-mCh Patch Intensity
Mean Intensity (a.u.)
Time (s)
myo1+ ends
myo1-S361A ends
I
Fim1-mCh Patch Intensity
Mean Intensity (a.u.)
Time (s)
myo1+ div site
myo1-S361A div site
J
Fim1-mCh Patch Intensity
Mean Intensity (a.u.)
Time (s)
myo1+ sides
myo1-S361A sides

Figure 6

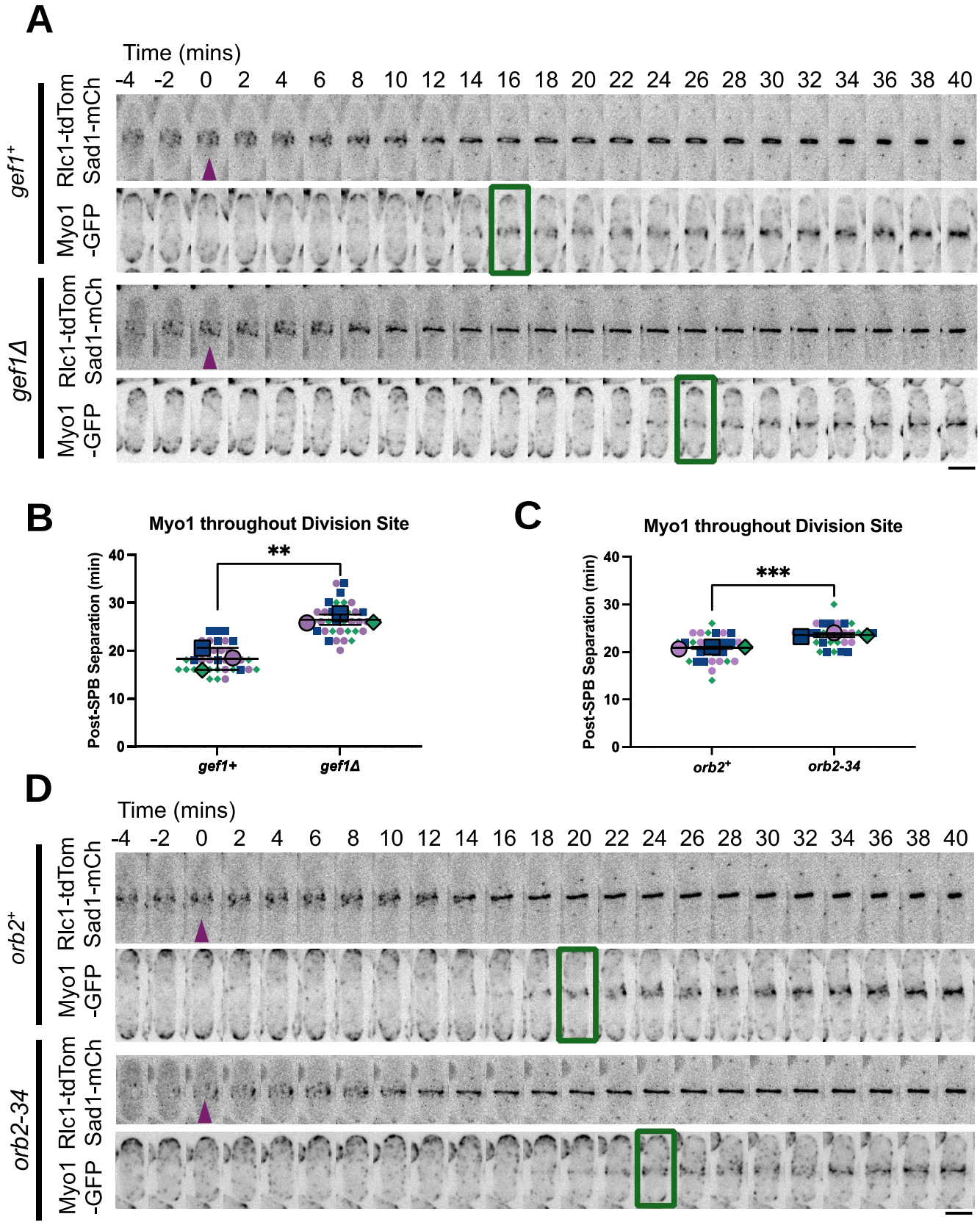
A
Time (mins)
-4 -2 0 2 4 6 8 10 12 14 16 18 20 22 24 26 28 30 32 34 36 38 40
gef1+
Rlc1-tdTom Sad1-mCh
Myo1 -GFP
gef1Δ
Rlc1-tdTom Sad1-mCh
Myo1 -GFP
B
Myo1 throughout Division Site
Post-SPB Separation (min)
0 10 20 30 40
**
gef1+
gef1Δ
C
Myo1 throughout Division Site
Post-SPB Separation (min)
0 10 20 30 40
***
orb2+
orb2-34
D
Time (mins)
-4 -2 0 2 4 6 8 10 12 14 16 18 20 22 24 26 28 30 32 34 36 38 40
orb2+
Rlc1-tdTom Sad1-mCh
Myo1 -GFP
orb2-34
Rlc1-tdTom Sad1-mCh
Myo1 -GFP

Figure 7

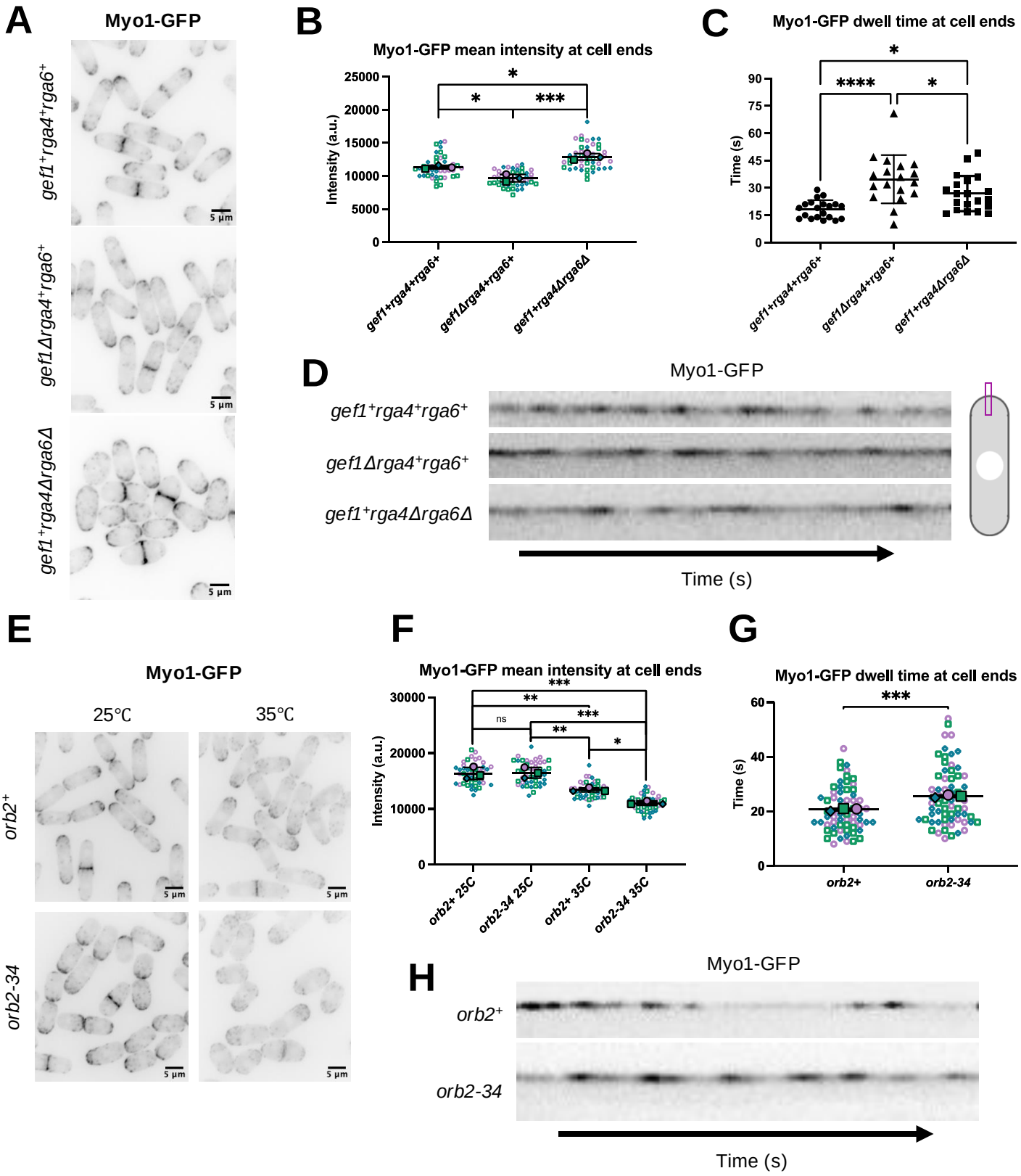
A
Myo1-GFP
gef1+rga4+rga6+
gef1Δrga4+rga6+
gef1+rga4Δrga6Δ
5 µm
B
Myo1-GFP mean intensity at cell ends
Intensity (a.u.)
25000
20000
15000
10000
5000
0
*
*
***
gef1+rga4+rga6+
gef1Δrga4+rga6+
gef1+rga4Δrga6Δ
C
Myo1-GFP dwell time at cell ends
Time (s)
90
75
60
45
30
15
0
*
****
*
gef1+rga4+rga6+
gef1Δrga4+rga6+
gef1+rga4Δrga6Δ
D
Myo1-GFP
gef1+rga4+rga6+
gef1Δrga4+rga6+
gef1+rga4Δrga6Δ
Time (s)
E
Myo1-GFP
25℃
35℃
orb2+
orb2-34
5 µm
F
Myo1-GFP mean intensity at cell ends
Intensity (a.u.)
30000
20000
10000
0
***
**
ns
***
**
*
orb2+ 25C
orb2-34 25C
orb2+ 35C
orb2-34 35C
G
Myo1-GFP dwell time at cell ends
Time (s)
60
40
20
0
***
orb2+
orb2-34
H
Myo1-GFP
orb2+
orb2-34
Time (s)

Figure 8